

# VISCOELASTIC SUPPORT JUNCTION DAMPING OF BEAMS

*T. J. MENDEL, R. L. SCHULTZ AND C. C. FU*

*UNIVERSITY OF MINNESOTA*

*MARCH 1961*

MATERIALS CENTRAL  
CONTRACT No. AF 33(616)-6828  
PROJECT No. 7351

WRIGHT AIR DEVELOPMENT DIVISION  
AIR RESEARCH AND DEVELOPMENT COMMAND  
UNITED STATES AIR FORCE  
WRIGHT-PATTERSON AIR FORCE BASE, OHIO

McGregor & Werner, Inc., Dayton, O.  
600 - October 1961 - 5-124 & 125

# *Contrails*

## FOREWORD

This report was prepared by the University of Minnesota, Department of Aeronautical Engineering under USAF Contract No. AF 33(616)-6828. The contract was initiated under Project No. 7351, "Metallic Materials", Task No. 73521, "Behavior of Metals". This work was administered under the direction of the Materials Central, Directorate of Advanced Systems Technology, Wright Air Development Division, with Mr. D. M. Forney, Jr. acting as project engineer.

This report covers a portion of work carried in the period June 1959 to September 1960.

The authors wish to express their thanks to Mr. S. H. Chi for his work in determining the mechanical properties of the No. 466 adhesive. Manuscript preparation was by Mrs. David E. Wilder.

WADD TR 60-779

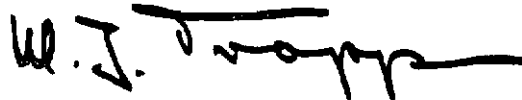
## ABSTRACT

An experimental study, together with evaluation of relevant theory, is conducted of the damping action at the support interfaces of beams which incorporate visco-elastic bonding material. The objective of the study is the identification of support junction damping techniques which might be of practical use in vibration attenuation. It is found that the highest energy dissipations are associated with flexure and rotation of the beam ends embedded within the support structure.

## PUBLICATION REVIEW

This report has been reviewed and is approved.

FOR THE COMMANDER:



W. J. Trapp  
Chief, Strength and Dynamics Branch  
Metals and Ceramics Laboratory  
Materials Central

# Contrails

## TABLE OF CONTENTS

SECTION		PAGE
I.	INTRODUCTION. . . . .	1
II.	INTRODUCTORY EXPERIMENTS. . . . .	1
III.	ARTICULATED MODELS FOR TRANSLATIONAL END MOTION.	4
IV.	DYNAMICAL RESPONSE OF BEAMS WITH TRANSLATIONAL END MOTION. . . . .	7
V.	ARTICULATED MODELS FOR ROTATIONAL END MOTION. . .	9
VI.	FLEXURAL DEFORMATION AT SUPPORTS. . . . .	13
VII.	DISCUSSION AND CONCLUSION . . . . .	14
	REFERENCES. . . . .	16

LIST OF FIGURES

FIGURE		PAGE
1	Beam with Viscoelastic Support Junction Damping . . . .	17
2	Properties of 3M No 466 Adhesive (Specific Batch Used in Experiments) . . . . .	18
3	Beam Specimens. . . . .	19
4	Beam Mounting . . . . .	19
5	Overall View of Experimental Set-Up . . . . .	20
6	Typical Results for Beam Specimens with Flared Ends . .	21
7	Comparison of Energy Dissipations at Supports . . . . .	22
8	Fundamental Modes . . . . .	23
9	Articulated Model Set for Translational End Motion. . .	24
10	Typical Results for Articulated Model . . . . .	25
11	Theory Versus Experiment for Steel Specimen 5B. . . . .	26
12	Theory Versus Experiment for Aluminum Specimen 6A . . .	26
13	Theory Versus Experiment for Aluminum Specimen 6B . . .	27
14	Dynamical Model for Response Calculation. . . . .	28
15	Amplitude Response of Steel Beam. . . . .	29
16	Amplitude Response of Aluminum Beam . . . . .	30
17	Adhesive Displacements. . . . .	31
18	Rotational End Motion Models. . . . .	31
19	Typical Results for Rotational Case, Large Quantity of Adhesive. . . . .	32
20	Typical Results for Rotational Case, Small Quantity of Adhesive. . . . .	33
21	Rotational Motion Dissipation Characteristics - 30 cps.	34
22	Rotational Motion Dissipation Characteristics - 45 cps.	35

# Contrails

## LIST OF FIGURES(cont.)

FIGURE		PAGE
23	Rotational Motion Dissipation Characteristics - 60 cps.	36
24	Rotational Motion Dissipation Characteristics - 75 cps.	37
25	Approximate Pressure Drop Off At Beam Sides . . . . .	38
26	Kinematical Model Incorporating Lateral Adhesive Displacements. . . . .	38
27	Frequency Shift of Dissipation. . . . .	39
28	Combinations of c and d for Maximum Dissipation . . . .	40
29	Flexural Deformation Support Damping Mechanism. . . . .	41
30	Exploded View of Set-Up for Flexural Deformation Mechanism . . . . .	41
31	Typical Results for Flexural Deformation Mechanism. . .	42
32	Influence of Geometry on Flexural Mechanism . . . . .	43

## LIST OF TABLES

TABLE		PAGE
I	. . . . .	3

## I. INTRODUCTION

Theoretical studies of vibrational energy dissipation at the support junctions of built-in beams and plates were reported in (1)\* and (2) and subsequently summarized and expanded upon by Mentel in (3). These studies, whose emphasis was on maximum damping, dealt primarily with the slipping at support interfaces together with the associated axial or membrane deformations. It was shown that such action could never result in strong damping for beams but that it could become an important contributor to the damping of plates. A few preliminary experimental tests (3), however, indicated that a set-up involving built-in supports, which was expected to attenuate all but the foregoing slipping action, was extremely sensitive to slight rotational motions whose damping action dominated all others.

The purpose of the present paper is to report a series of experimental results intended to throw more light on this damping behavior at built-in supports for beams which use a viscoelastic adhesive as bonding material. The ultimate objective of this work is to identify those mechanisms and relevant structural parameters, which would enable given damping action to be designed into support junctions of a structure. It is well known that, as yet, no satisfactory design approach to the damping in a structure has been developed. Extensive data is available on the selection of materials for machine elements which must rely solely on material damping. There has also been substantial development of theory for the treatment of damping coatings and sandwich construction for plates, but the visco-elastic support junction appears only now to have become a subject of (damping) study. For this reason the present investigation still follows an exploratory procedure.

The first section contains a description of the initial attempt at checking the theoretical results in (1). This experimental work serves as an introduction to the problem by demonstrating some unexpected damping characteristics of viscoelastic joints. The subsequent sections describe experimental testing with special models with the objective of developing a firm empirical basis on which either to test or formulate further theoretical work.

## II. INTRODUCTORY EXPERIMENTS

The series of experimental tests described herein was initiated to test the conclusions reached in (1). These conclusions pertained to the damping action due to small translational motions at the supports

---

\* Numbers in parenthesis refer to references in the Bibliography

Manuscript released by the author 13 October, 1960 for publication as a WADD Technical Report.

# Contrails

of built-in beams and plates. Some of the preliminary tests have already been described in (3), but these will be repeated here in order to make the present description complete.

The theory, as originally developed in (1), was concerned with the problem of augmenting damping in beam and plate structures where vibration of such structures made fatigue failure a critical problem. In particular, among the many well known techniques of incorporating damping into a structure, reference (1) was concerned specifically with the support junction mechanism. This mechanism is shown in Fig. 1 for the case of a built-in beam incorporating a viscoelastic adhesive as a bonding material. Attention was restricted to translational motion and axial deformation of the portion of beam in contact with the adhesive, and it was predicted that this purely translational motion was unlikely to produce important damping action, particularly as compared with inherent material damping or the sandwich type damping mechanisms. The case of the thin plate, however, using the same mechanism and similar theory, indicated that the translational mechanism, if suitably optimized, could provide a significant increase in damping.

The experimental study was directed first at the beam problem and was restricted to the case of viscoelastic bonds incorporated in built-in supports. The only viscoelastic adhesive readily available and easily worked with was type No. 466 made by the Minnesota Mining and Manufacturing Company. The material properties of this adhesive were interpreted by elastic and hysteretic stress coefficients  $G_1$  and  $G_2$ , as defined by the equation

$$\sigma = G_1 \gamma + \frac{G_2}{\omega} \frac{\partial \gamma}{\partial t} \quad (1)$$

where  $\sigma$  and  $\gamma$  are the shear stress and strain respectively and  $\omega$  is the frequency. A plot of these characteristics, using the parameters

$$G^* = \sqrt{G_1^2 + G_2^2}$$

and  $\tan \phi = G_2/G_1$  is shown in Fig. 2. The additional curves showing the temperature variation were constructed by linear interpolation between only two sets of data and hence are not precise. No account was taken of humidity since humidity control was not available and the complicated time lag effects associated with this variable were also unknown. The consequence of these complicated material properties was that correlation with theory could not be expected to be precise, but it turned out that the results obtained were satisfactory.

In setting up the beam experiments, it was found that unusually long embedded lengths would be required in order to develop the predicted optimum damping characteristics. This was due to the low stiffness of the adhesive and a minimum, accurately controlled thickness of bond of about 0.0015 inches, which the precision of the apparatus would permit. The beam ends were therefore flared out in order to give a large area on which to apply the adhesive. This design also provided an



# Contrails

alternate means of varying the axial stiffness by altering the size of the flared area, and it was hoped that the additional flexural stiffness, beginning at the point of entry of the beam into the supports, would minimize bending effects. A photograph of two beam specimens is shown in Fig. 3. The cantilevered sections located at center span were designed to provide a low energy loss connection for the electromagnetic shaker.

The apparatus was assembled by building up a given thickness of adhesive on all four end faces of the beam, and then clamping it into the support structure shown in Fig. 4. The distance between the upper and lower blocks of the support structure was controlled by using steel spacers between the blocks on both sides of the beam. Machined edges along the blocks permitted a precise check of the total distance between upper and lower faces after all bolts were tightened. The adhesive was usually built up to 0.001 or 0.002 inches excess thickness so that proper contact was assured. The clamping pressure required to achieve the necessary flow of adhesive was only a small fraction of that ultimately applied by the bolts. The consequent rigidity of the support structure appeared fully up to requirements. An overall view of the experimental set-up is shown in Fig. 5.

A number of duplicate experiments indicated that the results were repeatable so that no direct checks were made to see that the final adhesive thicknesses at the upper and lower surfaces were equal. The advantage of the given design was its simplicity and the fact that four adhesive faces were tested simultaneously, thus providing a strong, inherent averaging feature.

The limitations of the available electromagnetic exciter did not allow useful testing at beam resonance, but excellent results were obtained at system resonance. This latter resonance occurred at a relatively low frequency (less than 100 cps as opposed to several 100 cps) due to the mass of the shaker system acting like an attached concentrated mass of beam center span. The system thus behaved like a one degree of freedom set-up, with the vibration closely resembling the beam fundamental mode. This turned out to be a desirable feature since an equivalent simplification had been made in the theory.

One of the series of initial test specimens was 2 A, B and C as listed in Table I.

TABLE I

Specimen	Span $l$ (in.)	Depth $h$ (in.)	Width $b$ (in.)	Average Equivalent End Area $b d$ (sq. in.)
2A	10.0	0.184	0.199	1.371
2B	10.0	0.184	0.205	1.440
2C	10.0	0.184	0.205	0.694

The predicted thickness of bond (made of No. 466 adhesive) for maximum energy dissipation by the translational end motion was less than 0.006 inches for all of the foregoing specimens. A typical set of results giving the energy dissipation per cycle versus center span displacement amplitude is plotted in Fig. 6. The important observation, strikingly evident in this plot, is that the variation is single valued for the whole test range, with no optimum point evident. In addition, the variation with amplitude is more like  $\delta^2$  rather than  $\delta^4$ , which would have been characteristic of the assumed damping mechanism.

A replot of the results of Fig. 6 together with those of additional tests is shown in Fig. 7. In this case the results shown are for a fixed amplitude, with the empirical plot corresponding to the total observed energy dissipation less the material damping (given by the curve for  $c = 0$  in Fig. 6). The theoretical plot corresponds to the case of translational end motion. The disparity between these results obviously implies that some other damping mechanism dominated the behavior.

Although the flared out beam ends were expected to attenuate rotational (or flexural) effects at the supports, precisely these effects were the source of discrepancy. An example of the relative magnitude of the rotational component occurring at the supports is shown in Fig. 8. The comparison is between the case of rigid clamping (no adhesive, solid friction contact) and viscoelastic fixation, with the fundamental mode for a uniform clamped beam being shown for reference. Flexural deformation is clearly seen to occur within the junction, thus producing an oscillatory variation in the thickness of adhesive. Since the adhesive could not be expected to compress, lateral displacements, implying additional horizontal shearing action, must take place. A relatively complicated damping mechanism is thus indicated. It was concluded that although the dissipative characteristics of a built-in joint with solid friction contact may be explained adequately by considering translational end motions alone, the same considerations lead to erroneous results if a viscoelastic adhesive is placed at the interfaces.

### III. ARTICULATED MODELS FOR TRANSLATIONAL END MOTION

The experiments described in the foregoing section indicated that slight flexural deformation of the beam at the supports could be associated with large energy dissipations. In order to test this observation, an articulated model was constructed such that the motions at the supports could be restricted to being either pure translational or pure rotational. This was achieved by making the beam segments, contacting the supports, out of heavy steel sections which could be restricted either to primarily translational or to rotational motion by the use of flex plates. Axial and flexural deformations at the supports, of course, were deliberately inhibited by this design.

The set up for the case of translational end motion is shown in Fig. 9. The flexible beams for this case had a free span of 7 inches and were securely attached (with screws and bearing plates) to the heavy cantilever sections.

Before going on to the experimental results, it is useful to incorporate certain improvements in the presentation of the theoretical results which have been noted since the appearance of (3). Consider an adhesive whose stress-strain law for shear deformation can be adequately represented by Equation 1, given suitable methods for correcting  $G_1$  and  $G_2$  for temperature and frequency. If this adhesive is used as the bonding agent for a beam as shown in Fig. 1, and if the beam is undergoing a sinusoidal vibration in its fundamental (transverse) mode at a frequency  $\Omega$ , then the energy dissipation at the supports per cycle of motion is given by

$$D_v^* \equiv \frac{D_v}{bh\ell E} = 18.9 \delta^4 \left\{ s \sinh 2rd^* + r \sin 2sd^* \right\} \div \left\{ 4 \left( \cosh 2rd^* + \cos 2sd^* \right) + 4 \left( r \sinh 2rd^* - s \sin 2sd^* \right) + (r^2 + s^2) \left( \cosh 2rd^* - \cos 2sd^* \right) \right\}$$

The method of obtaining the foregoing result, where  $D_v$  is the energy dissipation per cycle and  $D_v^*$ , the dimensionless counterpart, is outlined in (3). The modification introduced here is the clear distinction between  $\omega$  and  $\Omega$ , where, in the present problem,  $\omega = 2\Omega$ . This has the effect of altering the definitions of some of the dimensionless parameters  $r$ ,  $s$ , and  $d^*$ , which are given by

$$r = \sqrt{\frac{e\ell^2}{ch} (1+m)} \quad , \quad s = \sqrt{\frac{e\ell^2}{ch} (1-m)} \quad , \quad d^* = \frac{d}{\ell}$$

where in turn, we now have

$$e = \frac{\sqrt{G_1^2 + G_2^2}}{E} \quad , \quad m = \frac{G_1}{\sqrt{G_1^2 + G_2^2}} \quad .$$

This result takes into account the axial flexibility of the beam throughout its length including the portions embedded within the supports (or flexibility of the joints). However, the axial flexibility of the joint was shown (3) to have a negligible influence on the damping for practical design geometries, and of course, it would be entirely absent in the articulated design shown in Fig. 9. This flexibility is therefore neglected with a marked simplification in the results. Thus, following the method of (3), the axial force in the beam for the case of the model in Fig. 9, can be written

$$N = \frac{2bdG_1}{c} s + \frac{2bdG_2}{\omega c} \frac{ds}{dt} + Ks + M \frac{d^2s}{dt^2}$$

# Contrails

where the last two terms have been added to account for the spring force and inertia associated with the cantilever sections and their flexplates. The width, length and depth of the bonds are given by  $b$ ,  $d$ , and  $c$  respectively. The translational (rigid body) displacement of the ends (cantilever sections) is given by  $s$ . The solution for  $s$  is readily obtained upon assuming a suitable vibratory motion for the beam and taking into account its axial deformation over its free span. The energy dissipated per cycle of transverse motion in the fundamental mode, is subsequently found to be

$$D_r = \frac{18.7 b d \ell^2 G_2 \delta^4 c^{-1}}{\left[ 1 + \frac{d \ell G_1}{c h E} + \frac{K \ell}{b h E} - \frac{2 \Omega^2 M \ell}{b h E} \right]^2 + \left[ \frac{d \ell G_2}{c h E} \right]^2} \quad (2)$$

The last two terms in the first square bracket are the additional ones resulting from the modification of the model as compared to that in (3). These terms, however, are found to amount to less than 10 percent of the  $d \ell G_1 / c h E$  term for typical sets of numerical values, and hence are dropped from the subsequent calculations.

Returning to the experiments, a typical set of measurements for the dissipation is shown in Fig. 10. A series of final reductions from a number of such sets of measurements for four different set-ups is given in Fig. 11, 12 and 13, together with the predictions of the foregoing theory. Some disparity is noted between theory and experiment, but in view of the nature of the material properties of the adhesive, these results were considered as providing a satisfactory demonstration of the validity of the theoretical analysis for the translational mechanism.

If the translational mechanism is suspected to be operative in some design, and if maximum damping is sought, then there occurs the problem of selecting the relevant design parameters. In the previous papers, this selection was achieved through maximization with respect to the properties of the adhesive, i.e.,  $G_2$  with respect to  $G_1$ , or the loss tangent  $\tan \phi = G_2 / G_1$ . The reason for this was that only the maximum theoretical values of damping were of interest and this provided a convenient means for their evaluation. For the case of the beam (upon omitting the additional terms brought in for the articulated models), this procedure gives

$$2 G_2 \underset{(\text{max. } D_r)}{=} G_1 + \frac{c h E}{d \ell} \quad (3)$$

Now it is obvious that damping is maximized if we set  $G_1 = 0$ , i.e. we have a purely viscous adhesive. Equation 2 will then be maximized when we have

$$2 G_2 = \frac{c h E}{d \ell} \quad (4)$$

with  $G_1 = 0$ . However, in the case of a design problem, other considerations, such as environmental factors, may determine the adhesive properties, so that it becomes necessary to optimize the geometry. If the thickness of the adhesive is taken as a variable parameter, then

$$\frac{c}{l} \underset{(\text{max. } D_r)}{=} = \frac{d}{hE} \sqrt{G_1^2 + G_2^2} \quad (5)$$

It is now observed that the (optimized) expressions (3) and (5) for maximum damping will give different values for the energy dissipation. Only expressions (4) and (5), together with the requirement of  $G_1 = 0$ , give the same result. This fact of the relative maximum (for a function of several variables) was not pointed out in the previous reports, nor the role of Equation 5 as the preferred equation for design application.

#### IV. DYNAMICAL RESPONSE OF BEAMS WITH TRANSLATIONAL END MOTION

As a result of the successful analysis in the foregoing section of the translational motion situation, it was of interest to pursue this specific case to the dynamical response problem. A theoretical method of calculating the steady state response of beams with translational and rotational damping mechanisms at the supports was developed in (4). Approximate solutions to the nonlinear equations of motion were produced only for near resonance (fundamental mode) conditions, but these were sufficient to allow comparison with the present experimental results. Of the two techniques outlined in (4), the one employing a discrete model is chosen here on account of the simplicity with which it can be applied to the present case.

The dynamical model, in its simplest form, is shown in Fig. 14, where the concentrated, central mass has been added to account for the shaker attachment mass in the experiments. The development and solution of the equations of motion may be carried out step by step following (4), and hence will be omitted here. It is recorded here only that the hinges at C and D (Fig. 14) are assumed capable of allowing the adjacent rigid segments to both rotate and translate (axially) with respect to each other. This, of course, allows both the flexural and the axial stiffness of the beam to be accounted for.

After the development of the equations of motion, the introduction of specially formulated small parameters and the application of perturbation solution techniques, the frequency equation, up to orders of

# Contrails

$\lambda^2$ , is found to be

$$\omega^2 = \omega_0^2 (1 + 2\bar{\omega}_1 \lambda^2)$$

where  $\theta = \lambda x$  (so that  $\lambda$  is "smallness" parameter")

$\omega_0$  = fundamental natural frequency of the corresponding linear problem.

$\omega_1$  = The first term in the expansion  $\bar{\omega} \equiv \frac{\omega}{\omega_0} = \sum_0^{\infty} \bar{\omega}_n \lambda^{2n}$

The expression for  $\bar{\omega}_1$  is

$$\bar{\omega}_1 = 0.5 A^2 \left[ (a_0 + 0.5 b_0) \bar{r} + c_0 \bar{r}' \right] + 0.5 A^2 \left[ f^2 A^{-6} \lambda^{-4} - (b_0 \bar{r}' + 0.5 c_0 \bar{r})^2 \right]^{1/2}$$

where

$$\bar{r} = \frac{r}{\omega_0^2}, \quad r = \frac{3K_{AE}}{3M+m}, \quad \bar{r}' = \frac{r'}{\omega_0^2},$$

$$r' = \frac{3K'_{AE}}{3M+m}, \quad A = x(0), \quad f = \frac{3P}{l\lambda(3M+m)}, \quad a_0 = \frac{1}{2q},$$

$$b_0 = \frac{q}{8\rho^2 + 2q^2}, \quad c_0 = \frac{p}{4\rho^2 + q^2}, \quad \rho = \frac{3K'_{AE}}{K_{AC}}, \quad q = 2 + \frac{3K_{AE}}{K_{AC}}$$

Where in turn

- $K_{AE}, K_{AE}$  = The elastic and viscous axial spring constants at hinge E (which takes the place of the support junctions).
- $K_{AC}, K_{BC}$  = The elastic axial and bending spring constant at hinge C.
- $l$  = Beam span.
- $2P$  = Amplitude of applied excitation
- $2M$  = Concentrated central mass
- $2m$  = Beam mass

A comparison of theoretical and experimental results is given for the case of a steel and aluminum beam in Fig's. 15 and 16 respectively. The theoretical curves were computed for fixed values of

$$G^* = \sqrt{G_1^2 + G_2^2}$$

with  $G_1 = G_2$ . This, of course, was not true for the experiments where the adhesive material properties varied with frequency, environmental factors, etc. For this reason, two fixed values of  $G^*$  were chosen such that they could be expected to bracket the actual variation. The comparison shows the theory to be approximate, at best, but in view of the theory being only the first order solution for a grossly simplified model (both mathematical and physical approximations), the agreement is probably adequate.



Further study of the response problem, including the theoretical analysis based on a continuum model (4), is to be included in a later report.

## V. ARTICULATED MODELS FOR ROTATIONAL END MOTION

The preliminary experiments using the articulated models revealed that the damping action associated with the rotational case was substantially more complicated than that associated with the translational case. The initial conjecture was that the primary agency for this damping action was the shear stress in the adhesive which was set up by the pumping action of the rotational motion. A displacement pattern corresponding to such a motion is shown in Fig. 17. Only a two dimensional motion is depicted in this figure, although the actual motion must be three dimensional. The solution for this motion would be a major undertaking even if the full three dimensional stress strain relationships for the adhesive were known, but only the shear properties of the latter were available. For this reason, it was considered instructive to study elementary models which might help only to identify the basic mechanisms involved. In particular, it was of immediate interest to learn whether the aforementioned shear stresses were in fact the primary agents in the damping action.

A case considered was where the length of bond (d) is substantially smaller than its width (b) so that the two dimensional motion depicted in Fig. 17 might be applied. The gross simplification was then made of assuming the displacement profiles to be parabolic. The main attraction for this simplification stems from the small total thickness of adhesive, but of course, this isn't sufficient reason even to rule out boundary layer effects, whose influence could be controlling. It is recalled, however, that in many instances of viscous flow, variations of flow profile are associated only with secondary effects. The specific example of the two dimensional, slow motion of a viscous fluid as it is forced out from between two parallel plates while the latter are being brought together, does give rise to parabolic displacement profiles. Nevertheless, choosing a specific profile implies specific variations of dissipative properties with thickness, which thus cannot be expected to be correct. It is not evident, however, that the gross dissipative characteristics should be invalidated. The subsequent analysis, thus, which cannot attain either rigor or elegance, serves merely to test the foregoing conjecture of a simplified kinematical model.

The several reversals in the direction of motion in Fig. 14 appear necessary from conditions of volume and pressure continuity. The assumption of a parabolic displacement profile gives

$$z = C(yh - y^2)$$

# Contrails

where  $h = c + \theta x$  for  $\theta \ll 1$ .

The condition that there be no dillilation or cavitation of the adhesive for the region ABCD indicated in Fig. 14, then gives

$$C = 3\theta (k^2 d^2 - x^2) / h^3 \quad 0 \leq x \leq kd$$

where  $kd$  is the station at which zero longitudinal displacement occurs. With the introduction of the dimensionless parameters

$$\xi = \frac{x}{d} \quad \eta = \frac{y}{h} \quad r = \frac{c}{d}$$

the expression for the longitudinal displacement becomes

$$z = \frac{3\theta d (k^2 - \xi^2) \eta (1 - \eta)}{(r + \theta \xi)}$$

which gives the longitudinal velocity as

$$u = \frac{dz}{dt} = \frac{3\theta r d (k^2 - \xi^2) \eta (1 - \eta)}{(r + \theta \xi)^2}$$

If this velocity is parallel to both upper and lower surfaces, then there must be a vertical component, a reasonable description of which is simply

$$v = \theta \eta u .$$

The equations of motion may now be formulated by applying boundary conditions in the form of pressure continuity equations. The pressure developed in the adhesive will have components corresponding to the strains and strain rates, and the assumption is made that the strain rate part alone, or viscous component, determines the motion sufficiently well to enable an estimate of the dissipative action. It is observed that the adhesive properties are such that  $G_2 > G_1$ , so that certainly the elastic component does not dominate, but the neglect of  $G_1$  entirely is an additional important simplification whose validity remains to be examined. Nevertheless, continuing in the spirit of the simple model, the absence of  $G_1$  implies a purely viscous adhesive so that the Navier-Stokes equations can be used. These equations are:

$$\rho u u_x + \rho v u_y = -p_x + \mu (u_{xx} + u_{yy})$$

$$\rho u v_x + \rho v v_y = -p_y + \mu (v_{xx} + v_{yy})$$



# Contrails

for the given coordinate system. On retaining only the viscous terms (the experiments were conducted at a relatively low frequency) we obtain

$$P_x \approx \mu(u_{xx} u_{yy}) = - \frac{6\mu r \dot{\theta}}{d(r + \theta \xi)^4} \left\{ \eta(1-\eta)(r^2 - 2r\theta\xi - 3k^2\theta^2) + (k^2 - \xi^2) \right\}$$

If the conditions  $r \ll 1$  and  $\theta \ll 1$  are applied, this result simplifies to

$$P_x = - \frac{6\mu r \dot{\theta} (k^2 - \xi^2)}{d(r + \theta \xi)^4}$$

also,  $P_y \approx 0$

Similar results for the pressure gradients may be obtained for the remaining regions of the bond, and the value of  $k$  is established by requiring pressure continuity across the station  $x = kd$ . It turns out, however, that  $k$  is a variable given by an unwieldy expression. In order to remove this difficulty, it is necessary to neglect  $\theta \xi$  compared to  $r$ . This is valid when dealing with experimental results, for in all cases  $|\theta \xi|_{\max}$  was less than  $0.01r$ . With this approximation, the pressure distribution becomes

$$\begin{aligned} 0 \leq x \leq kd & \quad P = \frac{4\mu \dot{\theta} k^3}{r^3} \\ kd \leq x \leq \frac{d}{2} & \quad P = \frac{\mu \dot{\theta}}{4r^3} (1 - 12k + 16k^3) \end{aligned}$$

from which we find that  $k = 0.5/\sqrt{3}$ . The viscous resistive moment developed by the whole bond ( $-d/2 \leq x \leq +d/2$ ) is now easily evaluated and the energy dissipation per cycle is found to be

$$D_0 = 0.0378 \pi \mu d^5 b \omega \theta_0^2 c^{-3}$$

where the rotational motion is described by  $\theta = \theta_0 \cos \omega t$ . This result gives no hint of an optimum situation, but the first series of tests showed a striking maximization with respect to the variable  $d$ . For this reason, it was decided to expand the experimental program to allow a more detailed survey, and for this purpose a new series of models was constructed. Since only the rotational component was to be tested, the design of the models was kept simple as shown in Fig. 18. The general set-up of the four bonds was retained in lieu of designing a new support structure, although some means for a definite fixation of the axis of rotation would have been desirable.

Example sets of typical experimental results are shown in Figs. 19

# Contrails

and 20. A reduction of results from about fifty such sets of curves is shown in turn in Figs. 21, 22, 23 and 24. The occurrence of the maximum in the curves appears to be characteristic. Elastic deformation, which could give rise to such a behavior, had of course, been anticipated, and the stiffness of the beams and excitation linkage had been designed to ensure this would not enter. The observed phenomena therefore must involve either or both the material properties of the adhesive ( $G_1$ ,  $G_2$ ) and the geometry of the bond ( $b$ ,  $c$ ,  $d$ ).

The obvious item which would involve geometry would be the zero pressure in the adhesive along the sides of the beam. If the length to width ratio of the bond ( $d/b$ ) is less than one, then the associated lateral displacements in the adhesive might be looked upon as a local end effect. In this case, if we assume a simple linear drop off of pressure as shown schematically in Fig. 25, then the viscous moment, and hence total dissipation, would be reduced by approximately  $d/2b$ . Setting  $d/b = R$ , the resulting expression for the dissipation becomes

$$D_v = 0.0378 \pi \mu b^6 \omega \theta_0^2 c^{-3} R^5 (1 - 0.5R)$$

where, of course, the value of  $R$  must be less than 2. This expression clearly exhibits a maxima with respect to geometry in the qualitative sense of the experimental results.

The foregoing development suggests the possibility of an improved kinematical model, such as shown in Fig. 26. The lateral displacements have been chosen to vary linearly along the sides, although several other possibilities appear equally attractive. The volume and pressure continuity equations are easily obtained, but the first set of integrations introduce pronounced algebraic complexity. Further approximation, such as the assumption of linear pressure gradients (from point of peak pressure) but with the boundary displacement pattern of Fig. 26, leads to

$$D_v = 0.038 \pi \mu b^6 \omega \theta_0^2 c^{-3} R^5 (0.353 R^2 + 1)^{-1}$$

which indicates a reduction in the exponent from 5 to 3 as  $R$  increases, but otherwise does not display a maxima property.

A successful description of the damping mechanism by means of a simplified kinematical model thus does not appear easily arrived at. If the main source of difficulty results from the presence of lateral strains in the adhesive, then the corresponding problem for plates, where this motion would be absent, should be easier to handle. On the other hand, the variation with the adhesive thickness ( $c$ ) is also in marked disagreement, as had been anticipated. The dissipation predicted by the theoretical model exceeds the experimentally measured values by as much as two orders of magnitude. Two possible sources of this discrepancy are the assumption of parabolic displacement profiles and the

simplified solution of the equations involving the neglect of the momentum and elastic terms. The absence of any characteristic change in the experimental results from 30 cps to 75 cps, in which range the inertia forces increase by a factor of 5, would appear to support the neglect of the latter. There is some general shift of the curves with frequency, which is shown in Fig. 27. This shift, however, appears to be due solely to the frequency sensitivity of the material properties of the adhesive, the corrections for which have not been incorporated into the results shown. The indication, thus, is that if the shear mechanism is valid, then the assumption of parabolic displacement profiles is grossly in error. In conclusion, the foregoing analysis appears only to identify a case where the application of elementary (kinematical) models leads to erroneous results.

A plot of the experimentally observed combinations of  $c$  and  $d$  for maximum energy dissipation is given in Fig. 28. This plot shows that

$$\left. \frac{d^5}{c} \right|_{\substack{\text{(optimum} \\ \text{combination)}}} = \text{Constant} = 5 \times 10^{-4} \quad \substack{\text{(for given} \\ \text{experiments)}$$

which can be put in the dimensionless form

$$\left( \frac{d}{b} \right)^5 \times \left( \frac{b}{c} \right)^2 = 5 \times 10^{-4} .$$

No theory has yet been produced which yields such a result.

## VI. FLEXURAL DEFORMATION AT SUPPORTS

The tests described in the first section showed that local flexural deformation at the supports could play an important role in the energy dissipation mechanism. This suggests a design such as shown in Fig. 29, which incorporates the flexural action while at the same time retaining the stiffness and structural integrity of a rigid, built-in joint. In view of the results of section 4, dealing with the effect of lateral displacements, it would appear that such a design might be best exploited by a plate. This requires substantial new apparatus and has been made the subject of a separate report now in preparation. The present study is restricted to beams, with this specific section attempting to establish only the general characteristics of the given mechanism.

The steel beam specimen, shown in Fig. 30, was constructed with large ends to ensure secure damping deep within the support blocks. Special spacers were then added so that a variable length of beam located within the support blocks could be bonded with a given thickness of adhesive. The resulting cross section of the support structure, after assembly,

corresponded exactly to that indicated in Fig. 29.

A typical series of experimental results obtained with the foregoing set-up is shown in Fig. 31. A reduction from the combined results of four such series is shown in turn in Fig. 32. This reduction was made for the net energy dissipation at the supports (obtained by noting the energy dissipation for zero adhesive in Fig. 31 to be material damping) which occurs for a given center amplitude.

The results, as given in Fig. 32, show that the energy dissipation becomes maximum when the length of bond ( $d$ ) is about three times the beam width ( $b$ ). The situation for much stiffer adhesives, which is represented by the smallest thickness of bond ( $c$ ) in the present work, is less clear.

It is of interest to compare the results of Fig. 31 with those of Fig. 6. The earlier tests, in which all of flexure, rotation and translation took place at the supports, developed less than the maximum amount of damping obtainable by the flexural action alone. A partial explanation of this might be in the special shape of the ends of the beams in the early tests, which were flared out, and hence stiffer immediately at the support boundary, thus decreasing the flexural component.

The theoretical studies of this case have been restricted to include only the shear mechanism in the adhesive as the damping agent. However, in view of the somewhat simpler adhesive displacement which occurs in the corresponding case for circular plates, it was decided to study both cases together. Since this has not been completed, no theory is presented here.

## VII. DISCUSSION AND CONCLUSIONS

The main concern of this work has been to establish the optimum methods of vibration damping which might be incorporated into built-in support junctions. The initial theoretical work (1) was concerned only with translational motion which was associated with interface slipping. It was shown that in this case, the introduction of a visco-elastic adhesive between the interfaces (thus substituting viscous shear for solid friction), would always enable a greater energy dissipation to occur, when optimized conditions were compared. For this reason, experimental models with viscoelastic interfaces were designed, but it was discovered that even with thicknesses of adhesive of only two thousandths of an inch, an entirely different damping motion dominated the picture. This in turn lead to the special series of models reported herein.

One aspect of the basic characteristics of the viscoelastic support junction was found to be an optimization dependent on support geometry

alone in addition to optimization dependent on structural stiffness. This unexpected characteristic was apparently due to the influence of lateral displacements in the adhesive along the sides of the beam. An attempt at using a simplified kinematical model to provide an adequate explanation of this behavior proved unsuccessful, although some qualitative agreement was obtained. No attempt was made to carry through a more exact analysis, such as might involve computer solutions. Of several reasons for this, one was the lack of an adequate mathematical description of the damping properties of the adhesive under three dimensional deformation. The mechanical properties used in this paper were derived from (simple) shear tests.

The result of the foregoing situation was to limit the scope of the present work to establishing general characteristics only. An adequate theory remains to be developed. Certain important questions of engineering interest, however, were answered. These are as follows:

- 1) If a beam joint allows only interfacial slipping and solid friction applies, then the optimized (maximum) damping will at best only be of the order of magnitude of the maximum material damping. (The maximum material damping being obtained by optimum selection of beam material).
- 2) If a viscoelastic adhesive is introduced into the support joints, and if the design of the structure guarantees the end motion to be translational (so as to produce only pure shear at the interfaces), then the optimized damping will still be only of the order of maximum material damping, but it will be greater than that obtained by solid friction. (It should be noted that minimum material damping might be two orders of magnitude below these values).
- 3) If, in item 2 above, the restriction to translational end motion cannot be made, then rotation and bending of the beam within the support junction, even though so small as to require instrumentation to establish its presence, can give rise to about an order of magnitude increase in damping. A substantial volume of adhesive is required, as opposed to that needed for just achieving a bond, in order to make this mechanism effective. A simple design incorporating this mechanism is given in the paper.
- 4) Support junction damping for flexural beam vibrations, even when optimized, cannot be made as effective as other mechanisms such as sandwich core damping. (1)

The corresponding problem for plates, which might, equally well, be termed "boundary damping", does show some different properties and this has been made the subject of a separate paper (now in preparation).

## REFERENCES

1. Mentel, T. J., "Damping Energy Dissipation by Interfaces in Beam and Plate Supports and in Sandwich Cores", WADC Technical Report 58-547, December 1958
2. Mentel, T. J., and Fu, C. C., "Damping Energy Dissipation at Support Interfaces of Square Plates", WADC Technical Report 59-96, June 1959.
3. Mentel, T. J., "Vibrational Energy Dissipation at Structural Support Junction", Section 4 in "Structural Damping" edited by J. E. Ruzicka, ASME, 1959.
4. Fu, C. C. and Mentel, T. J., "Steady State Response of Beams with Translational and Rotational Damping Motions at the Supports," WADD Technical Report 60-60, 1960.

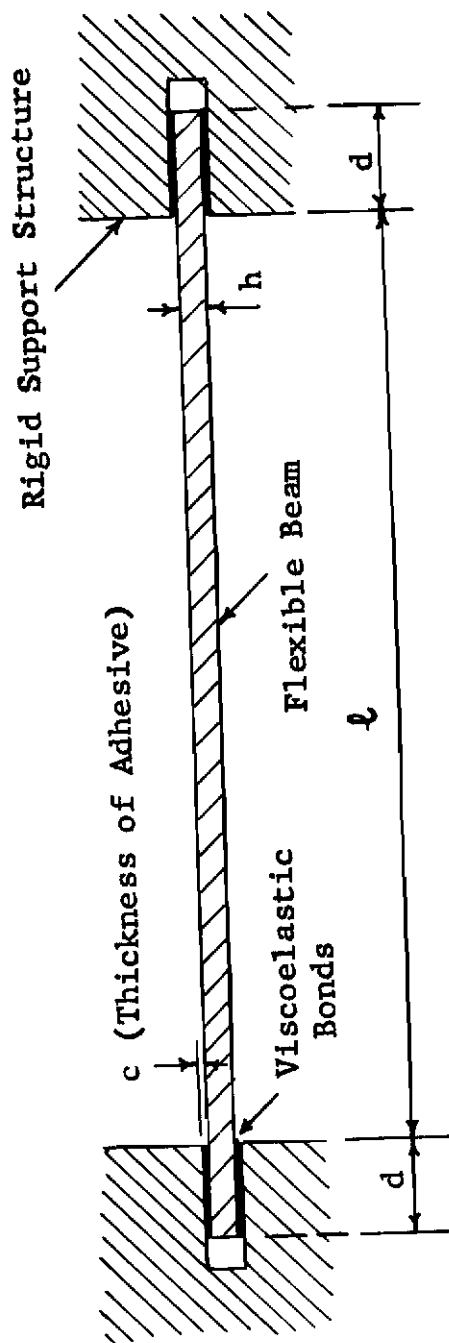


Figure 1 - Beam with Viscoelastic Support Junction Damping

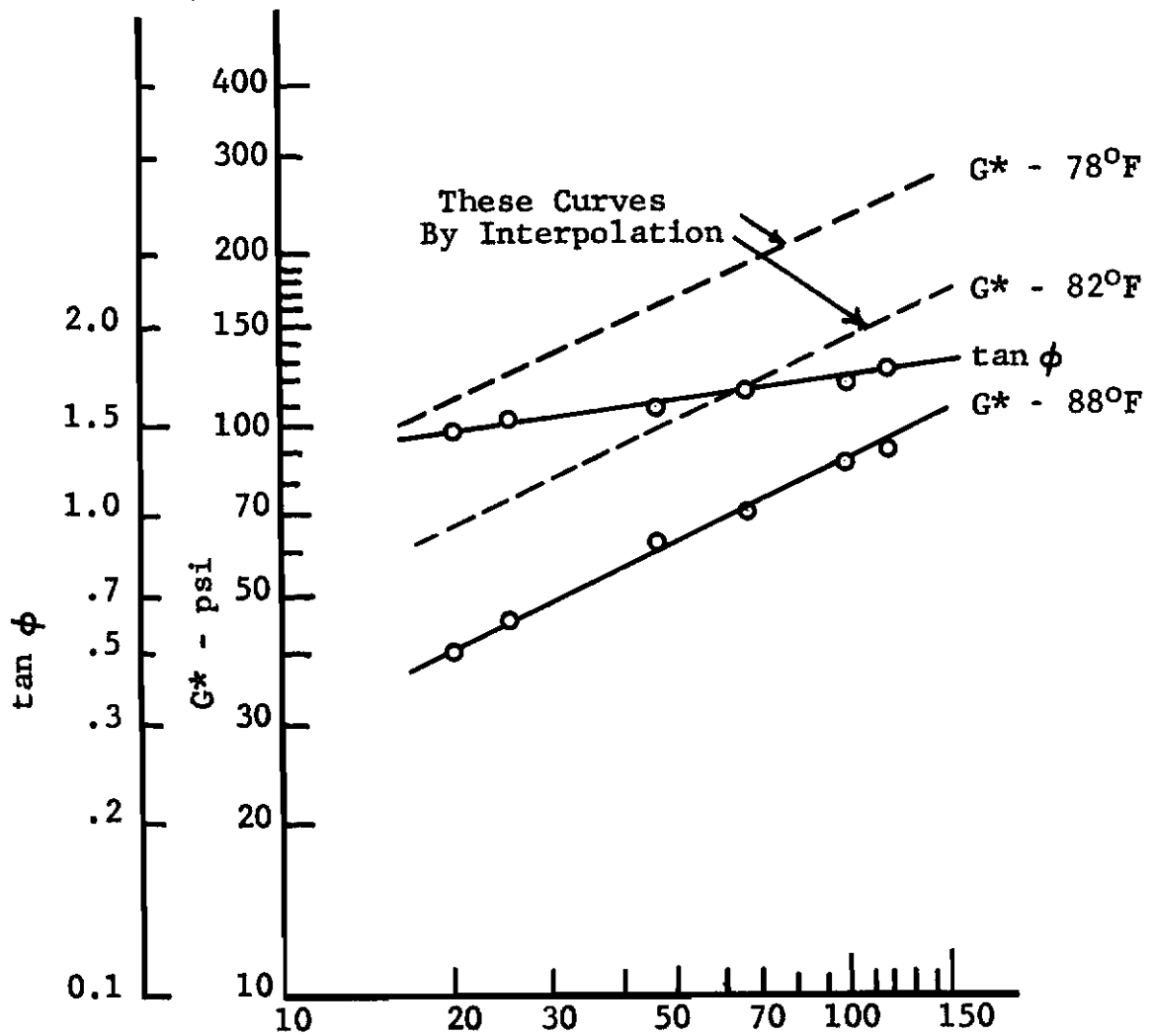


Figure 2 - Properties of 3M No 466 Adhesive  
(Specific Batch Used in Experiments)



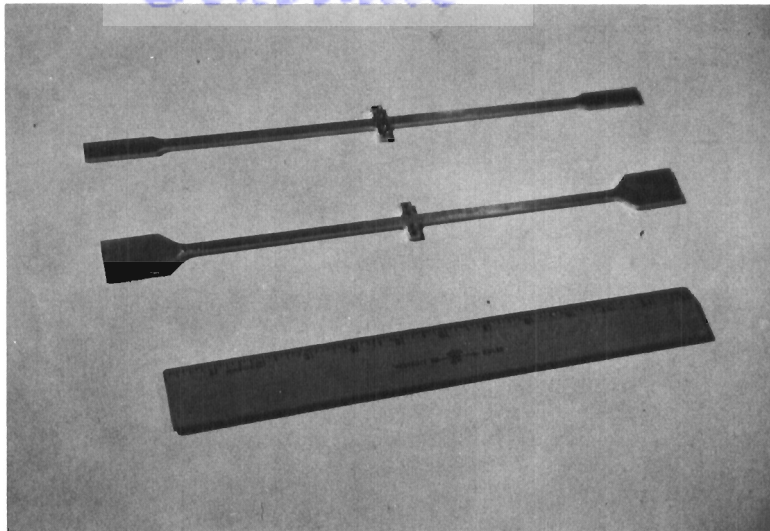


Figure 3 - Beam Specimens

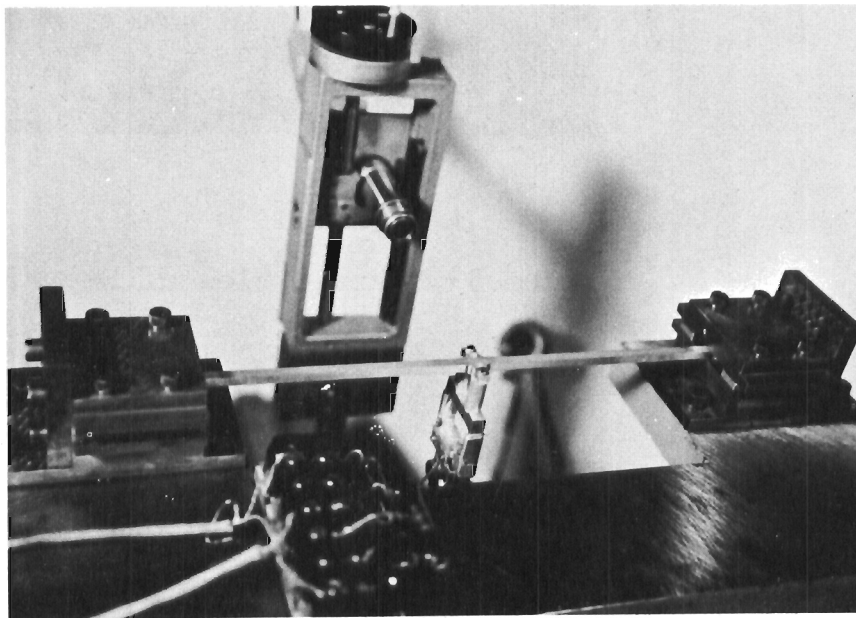


Figure 4 - Beam Mounting

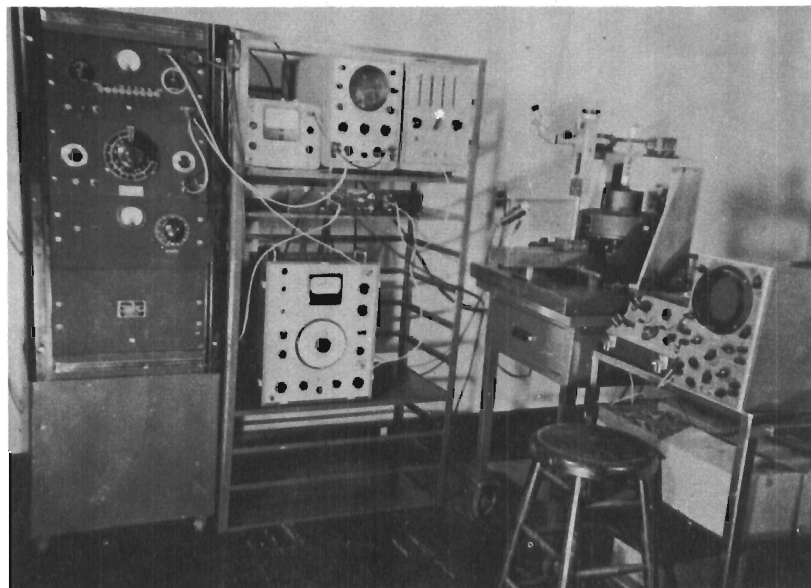


Figure 5 - Overall View of Experimental Set-Up

# Contrails

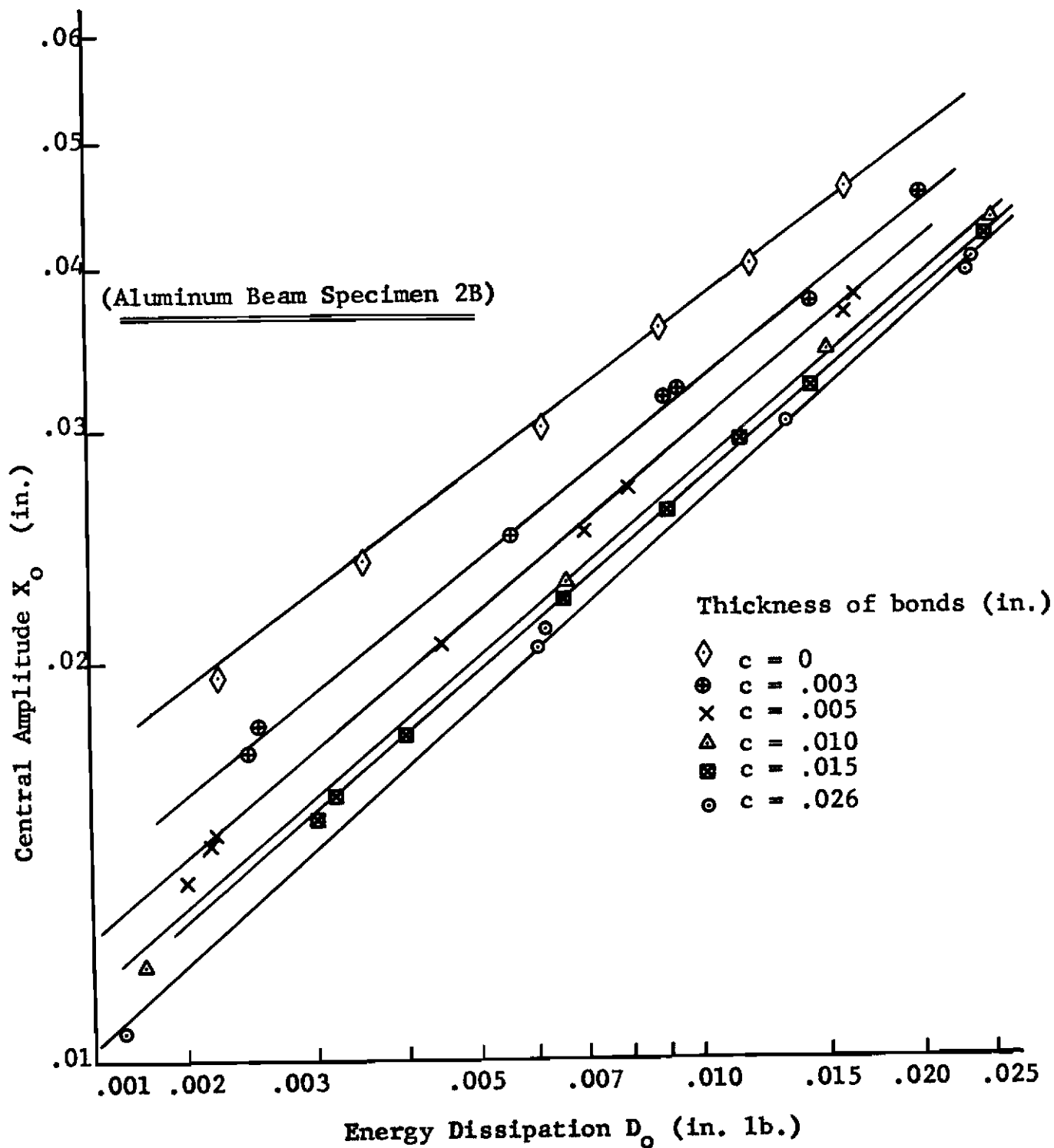


Figure 6 - Typical Results for Beam Specimens with Flared Ends  
WADD TR 60-779 21

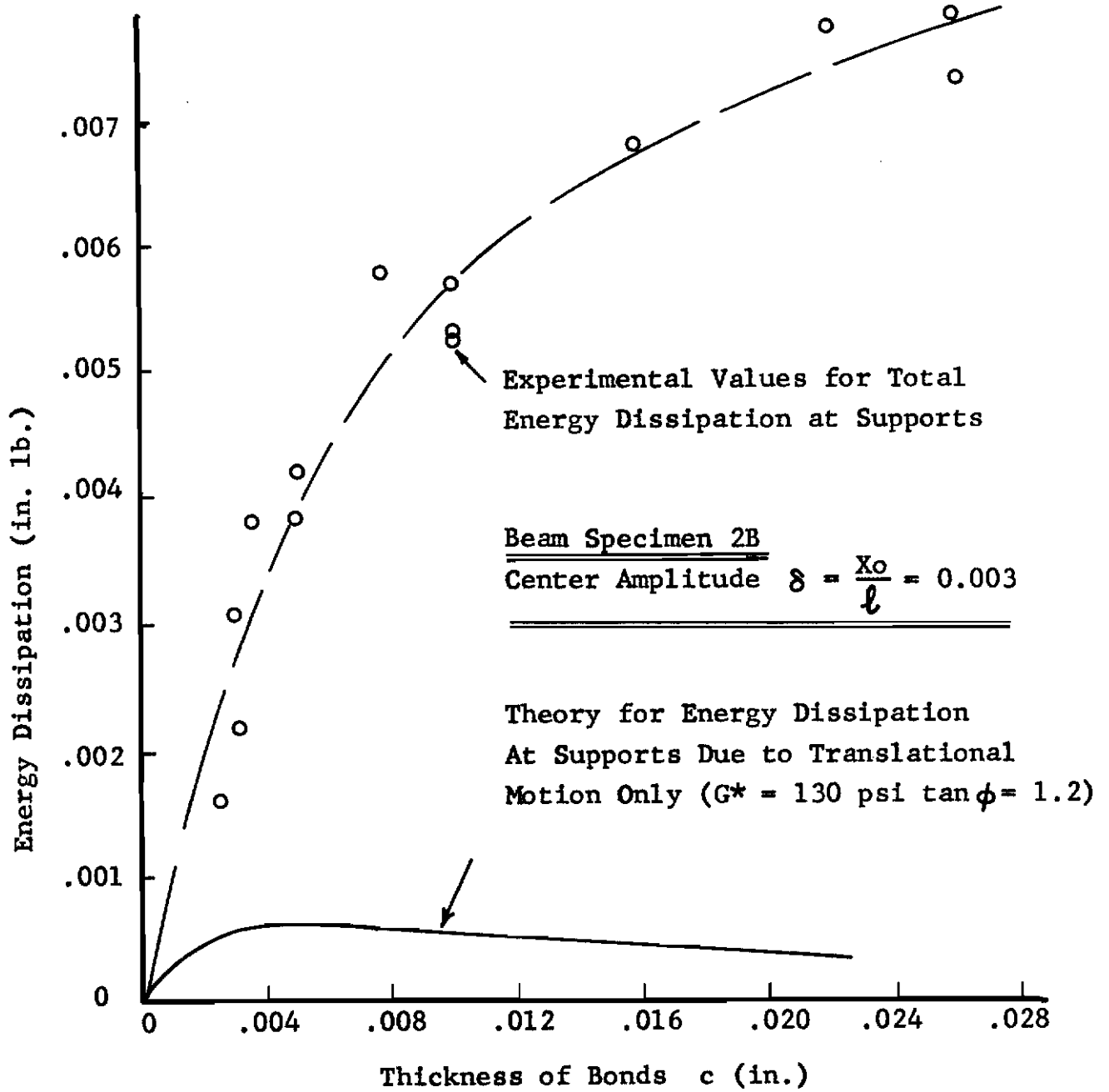


Figure 7- Comparison of Energy Dissipations at Supports

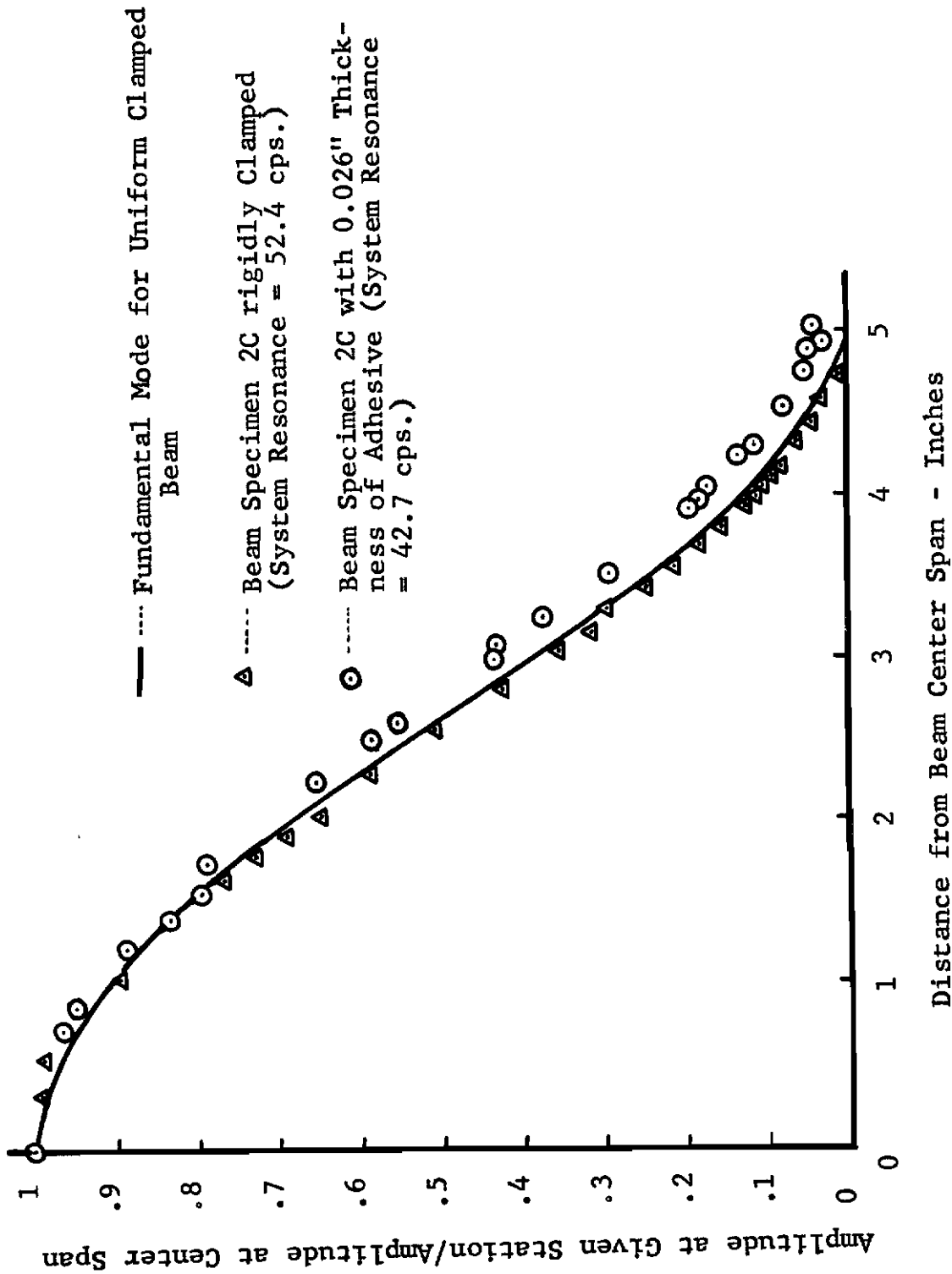


Figure 8 - Fundamental Modes

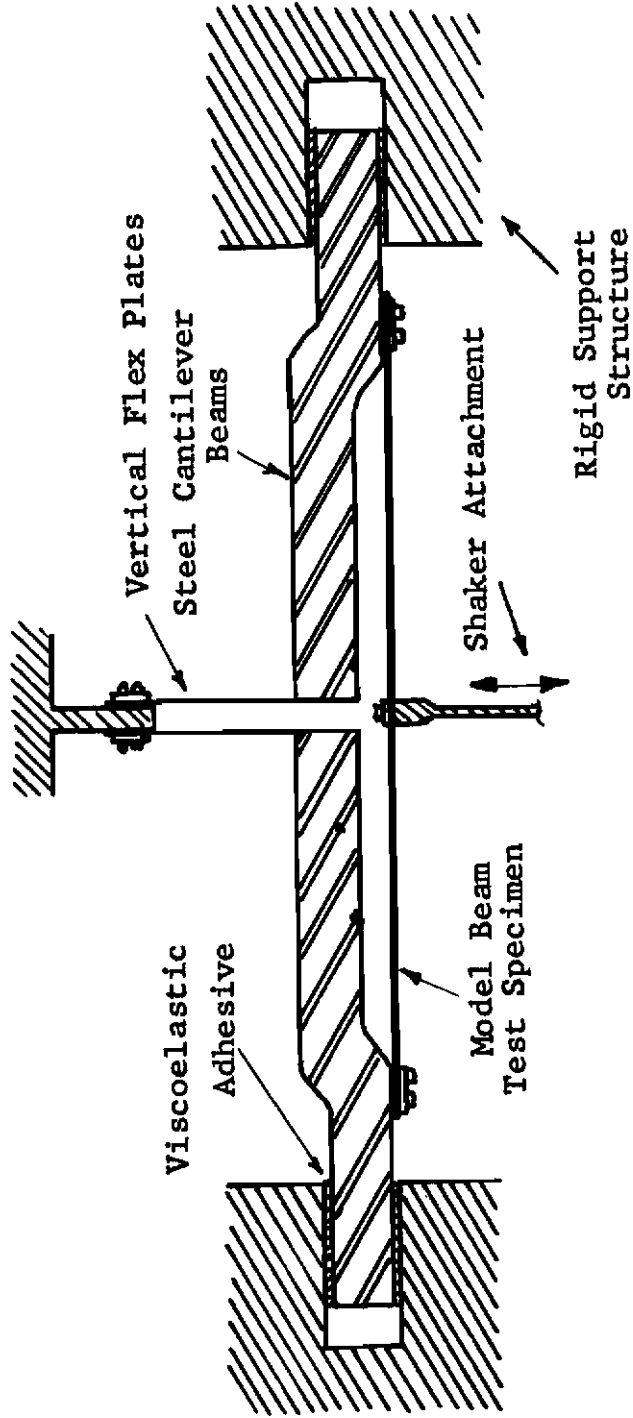
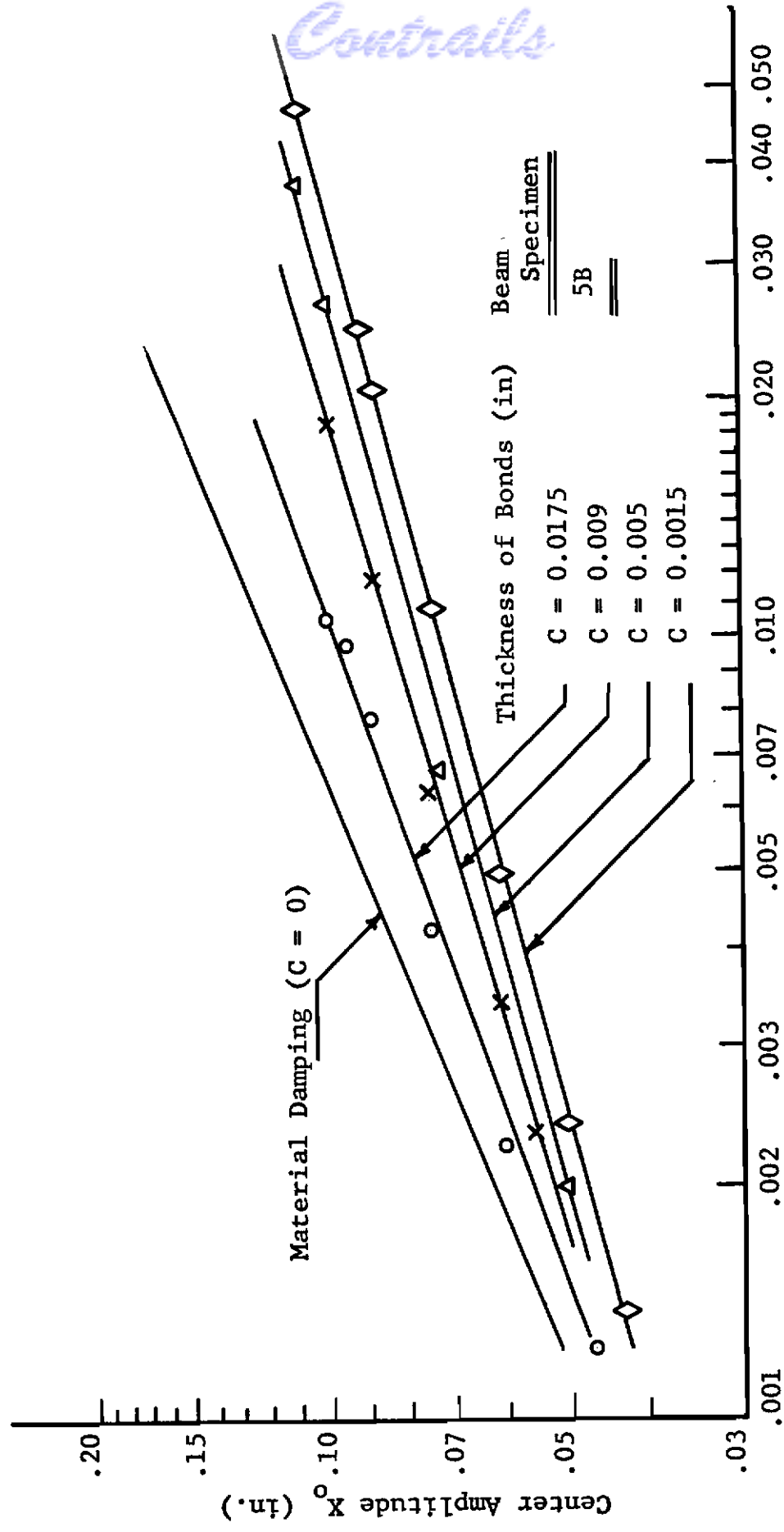


Figure 9 - Articulated Model Set for Translational End Motion



Energy Dissipation  $D_0$  (in. lb.)

Figure 10 - Typical Results for Articulated Model

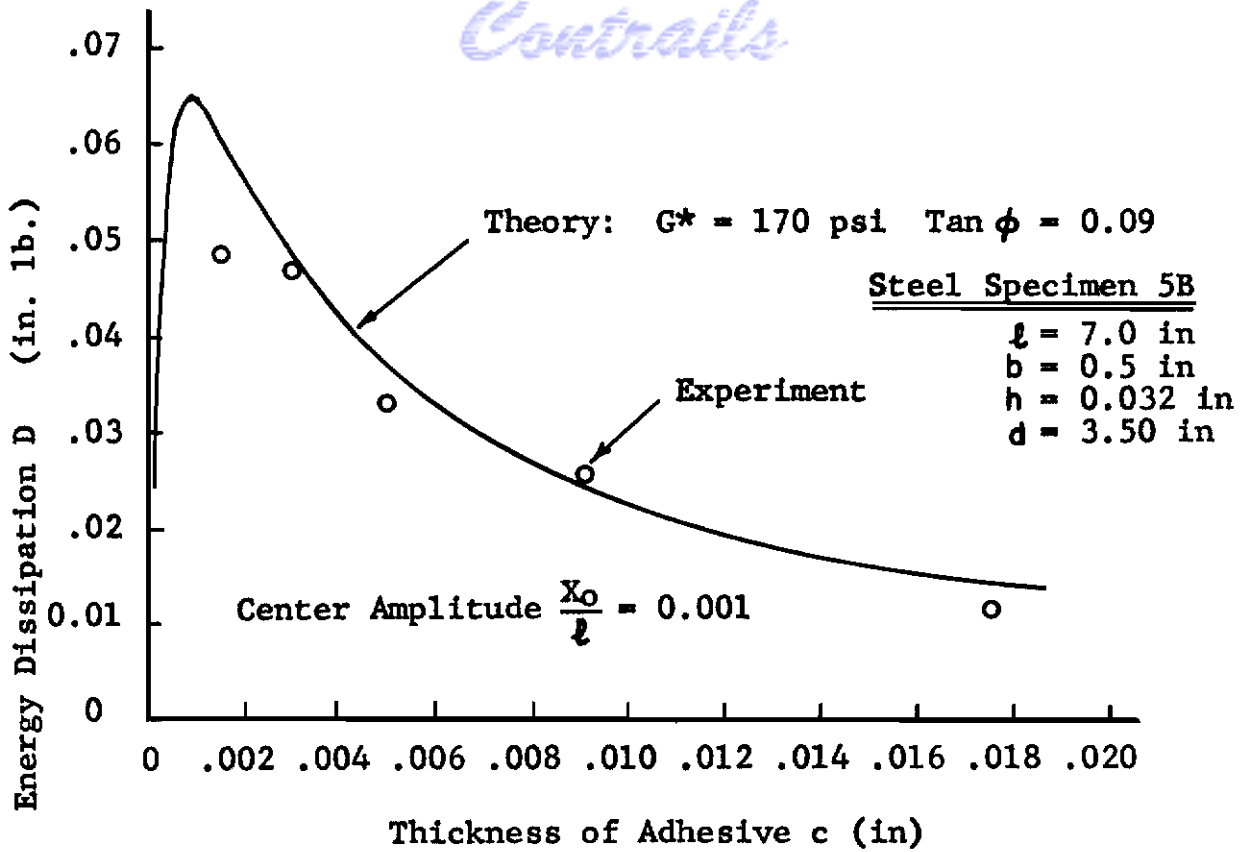


Figure 11 - Theory Versus Experiment for Steel Specimen 5B

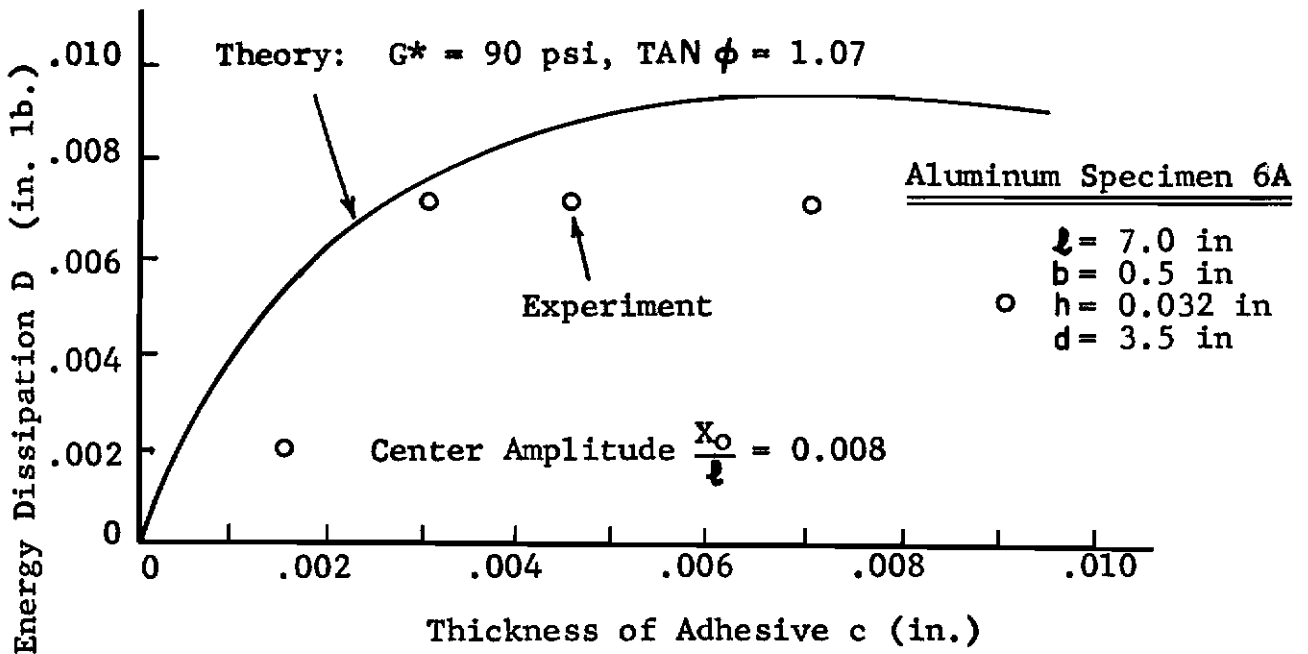


Figure 12 - Theory Versus Experiment for Aluminum Specimen 6A



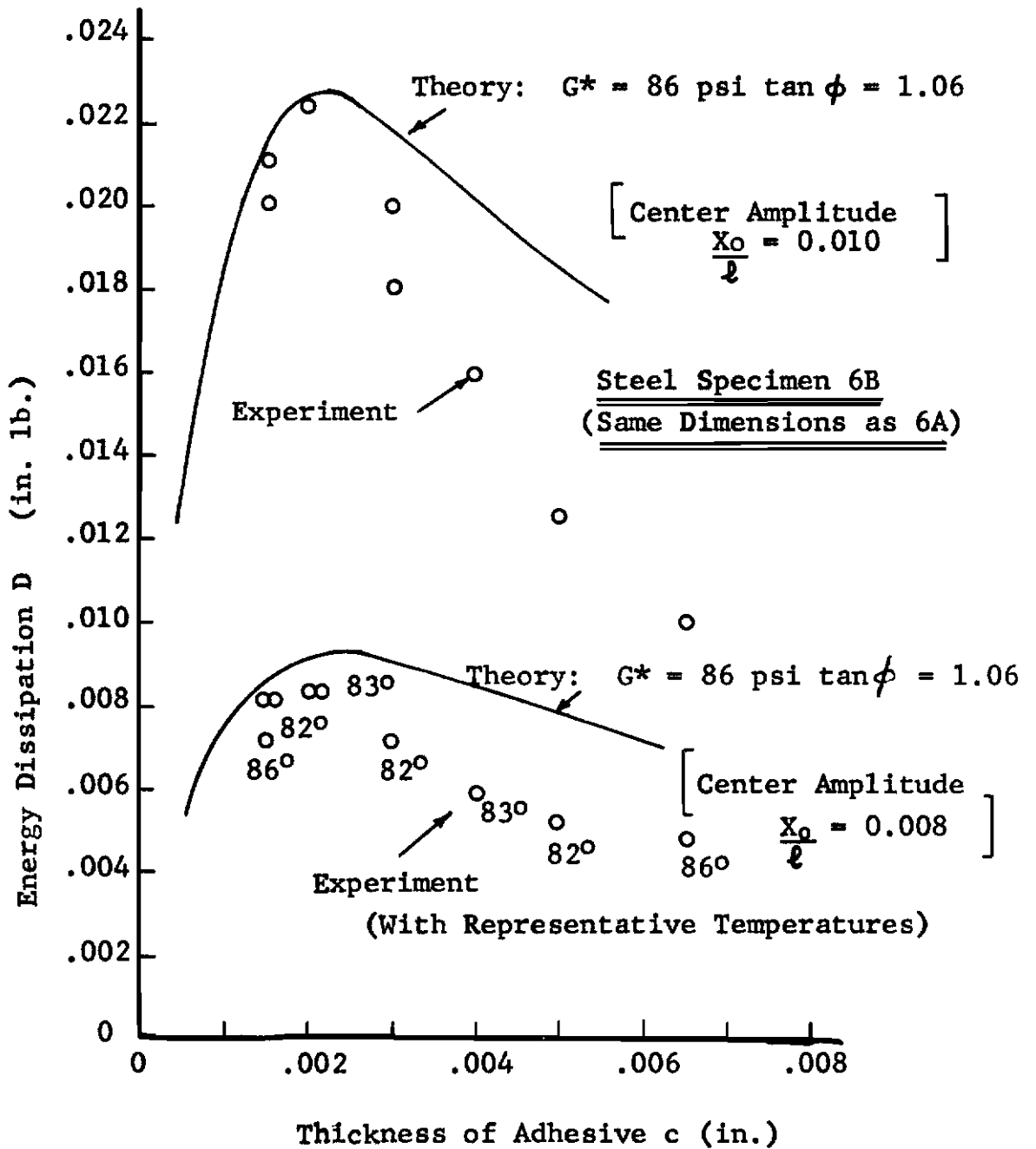


Figure 13 - Theory Versus Experiment for Aluminum Specimen 6B

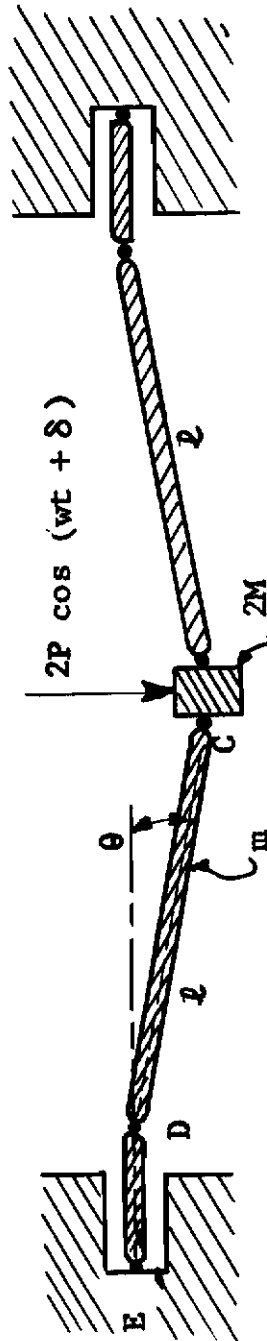


Figure 14 - Dynamical Model for Response Calculation

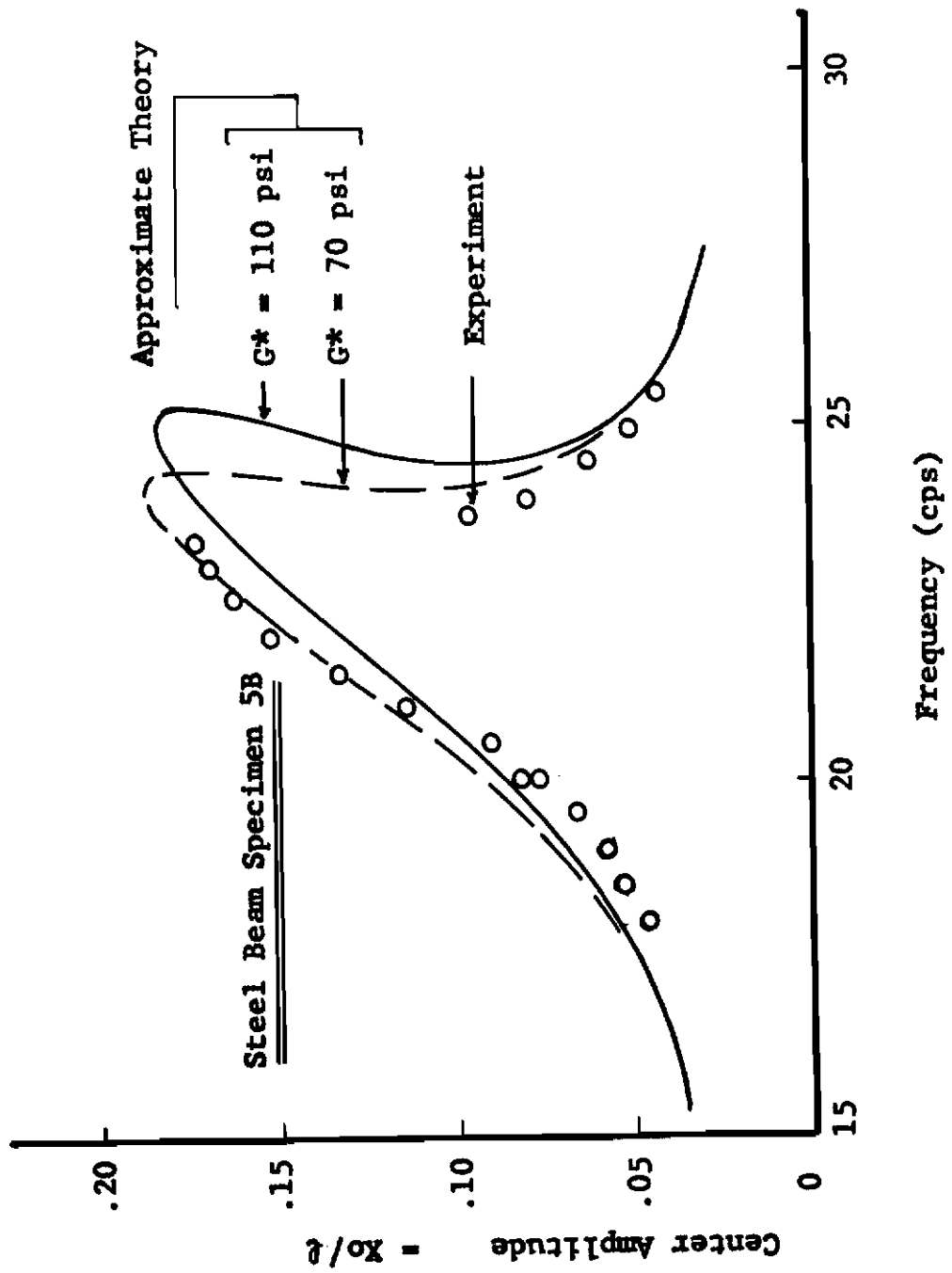


Figure 15 - Amplitude Response of Steel Beam

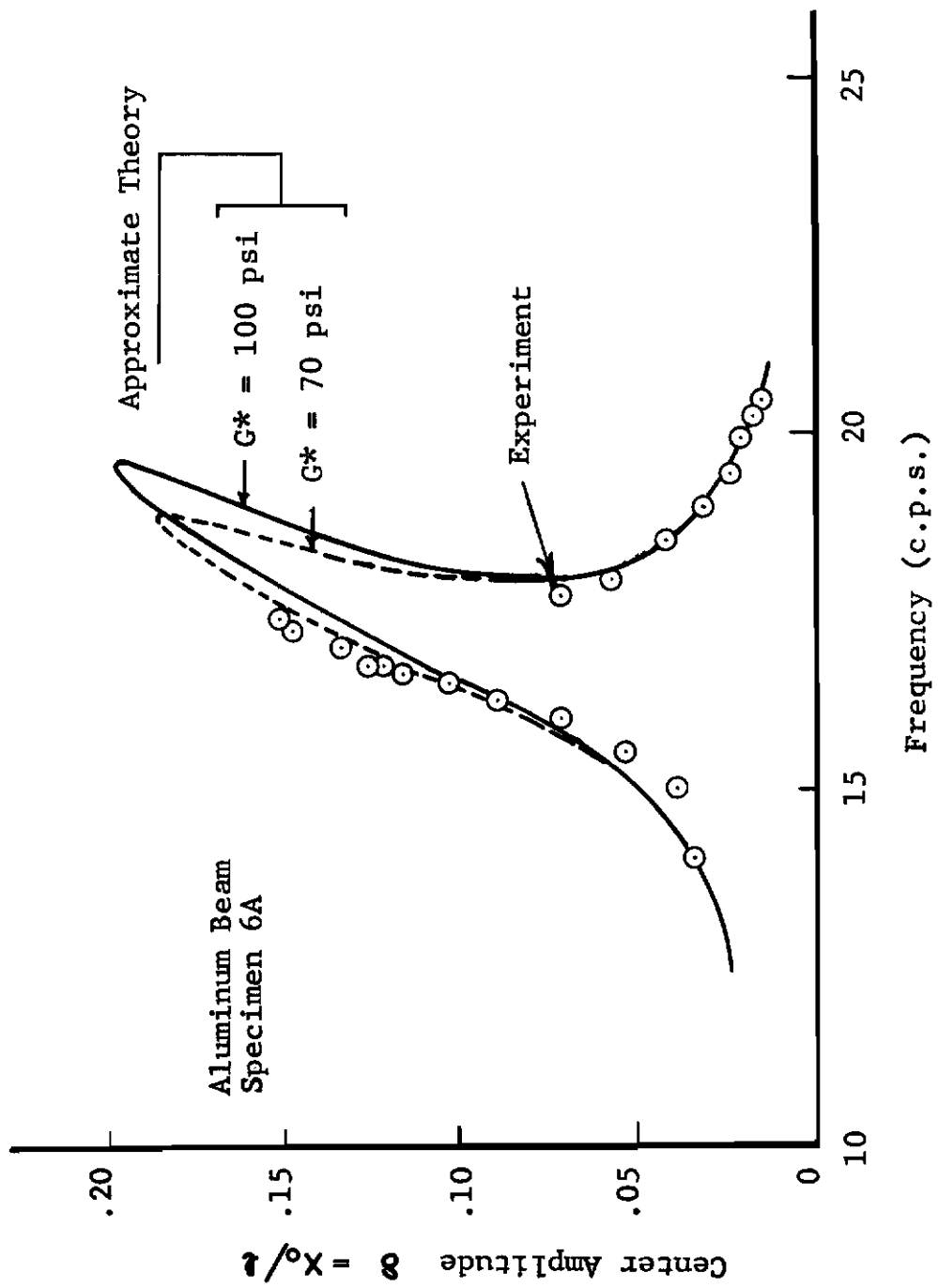


Figure 16 - Amplitude Response of Aluminum Beam

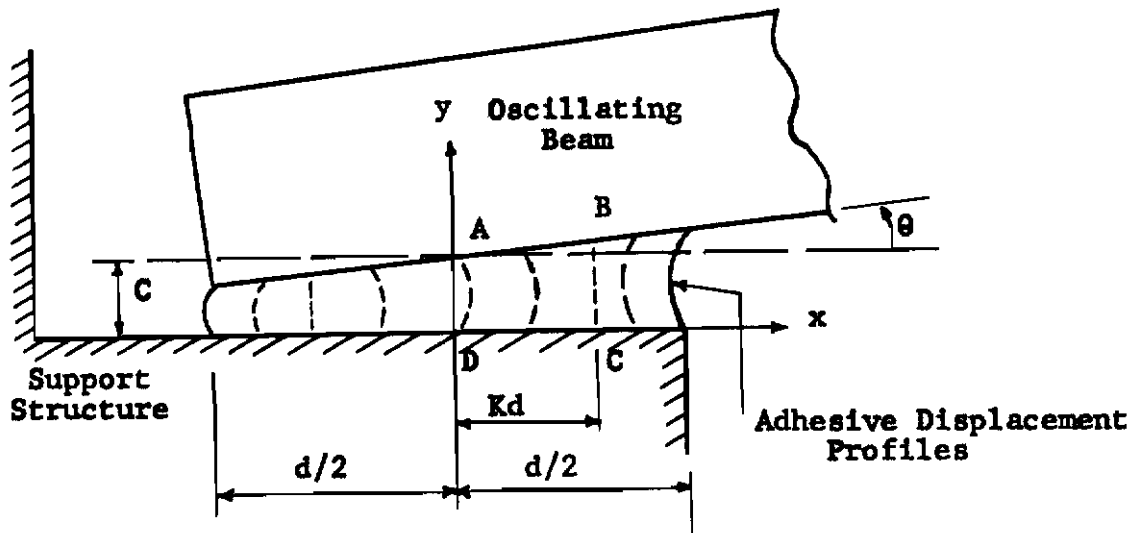


Figure 17 - Adhesive Displacements

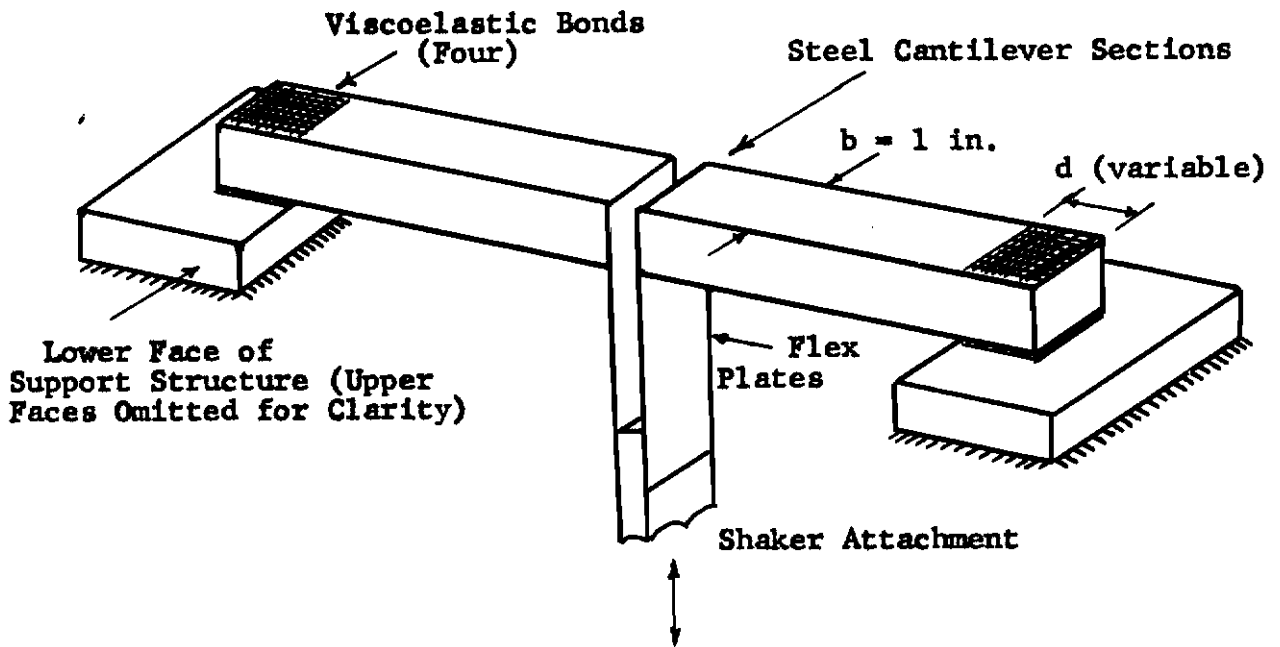


Figure 18 - Rotational End Motion Models

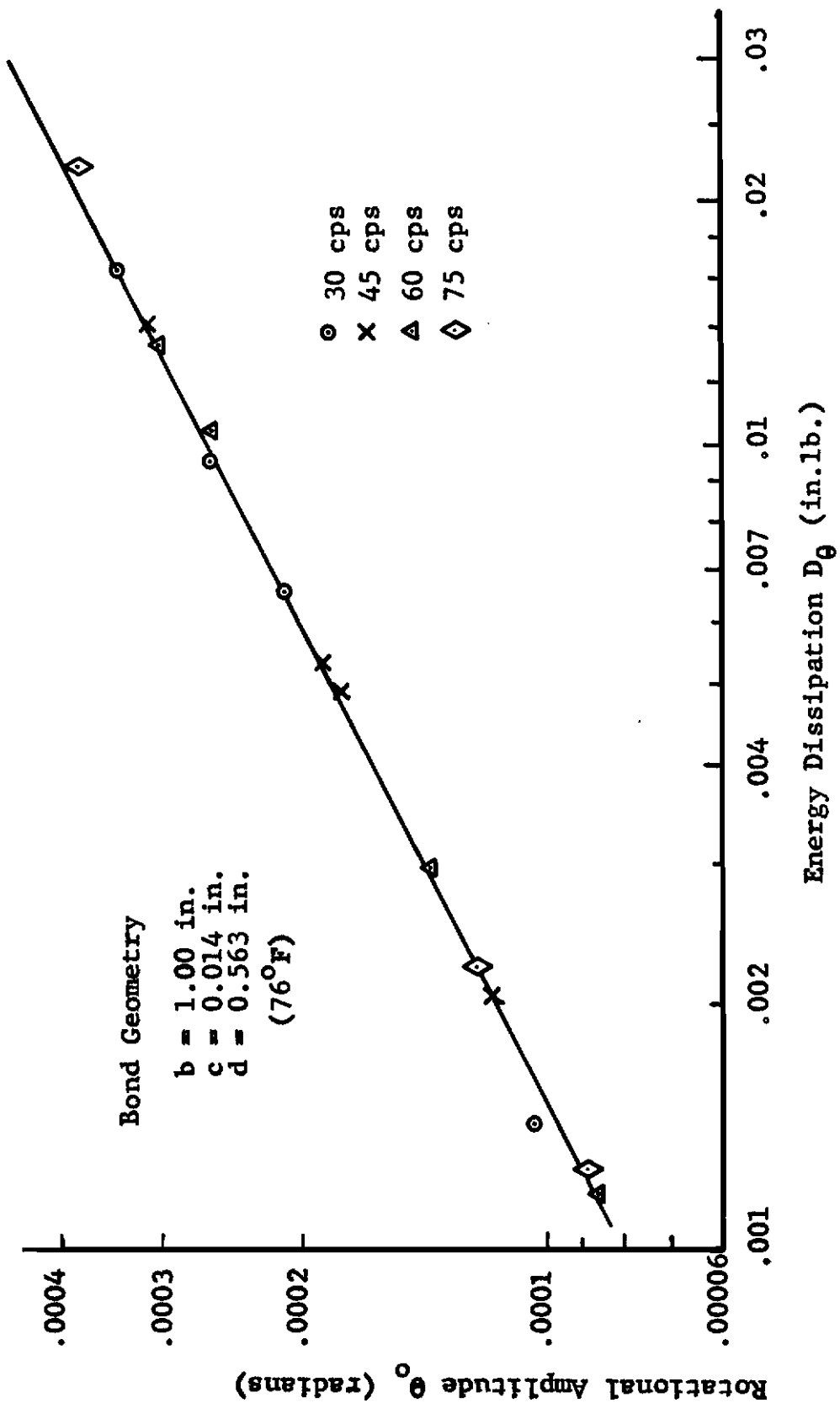


Figure 19 - Typical Results for Rotational Case, Large Quantity of Adhesive

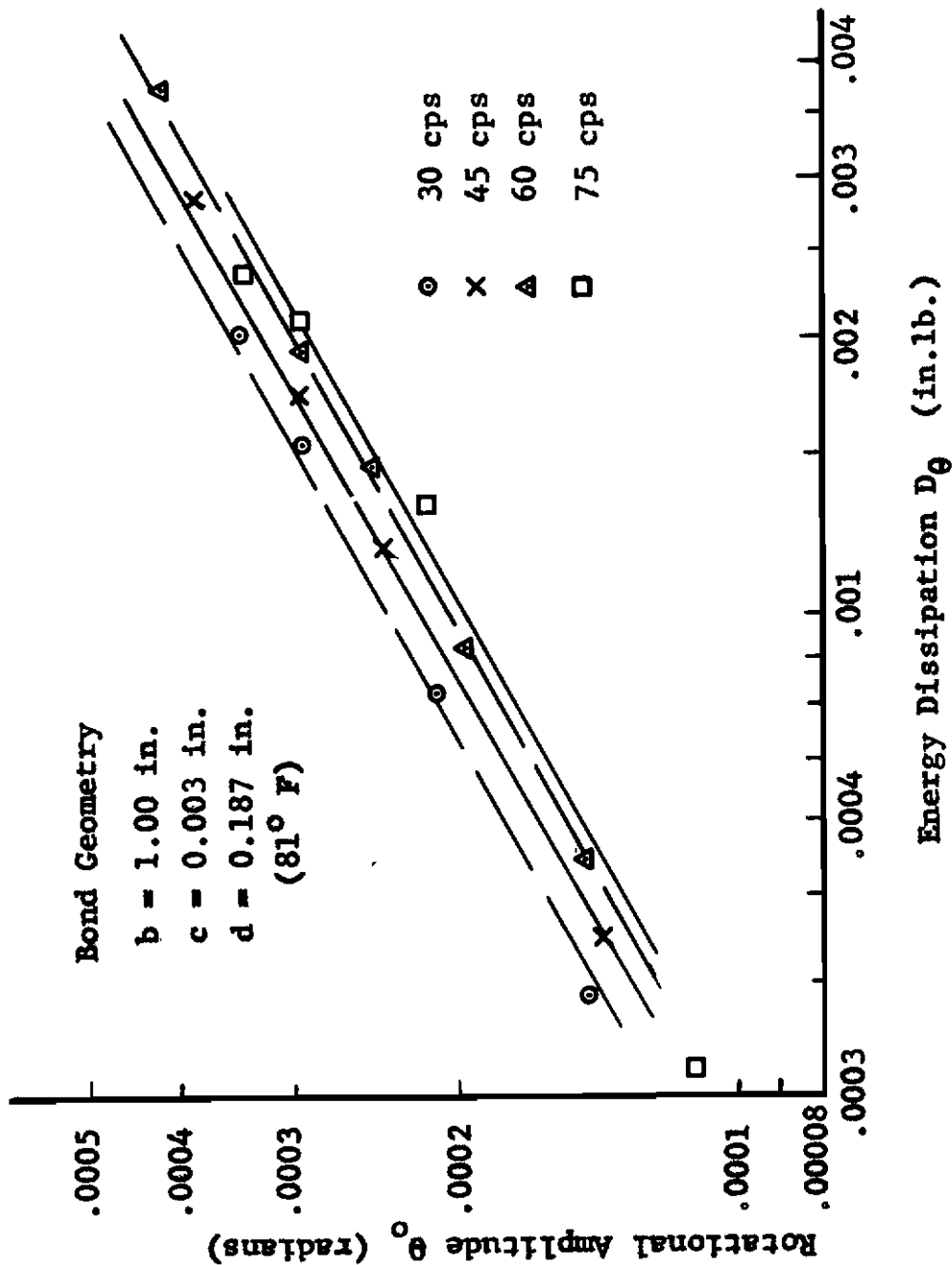


Figure 20 - Typical Results for Rotational Case, Small Quantity of Adhesive

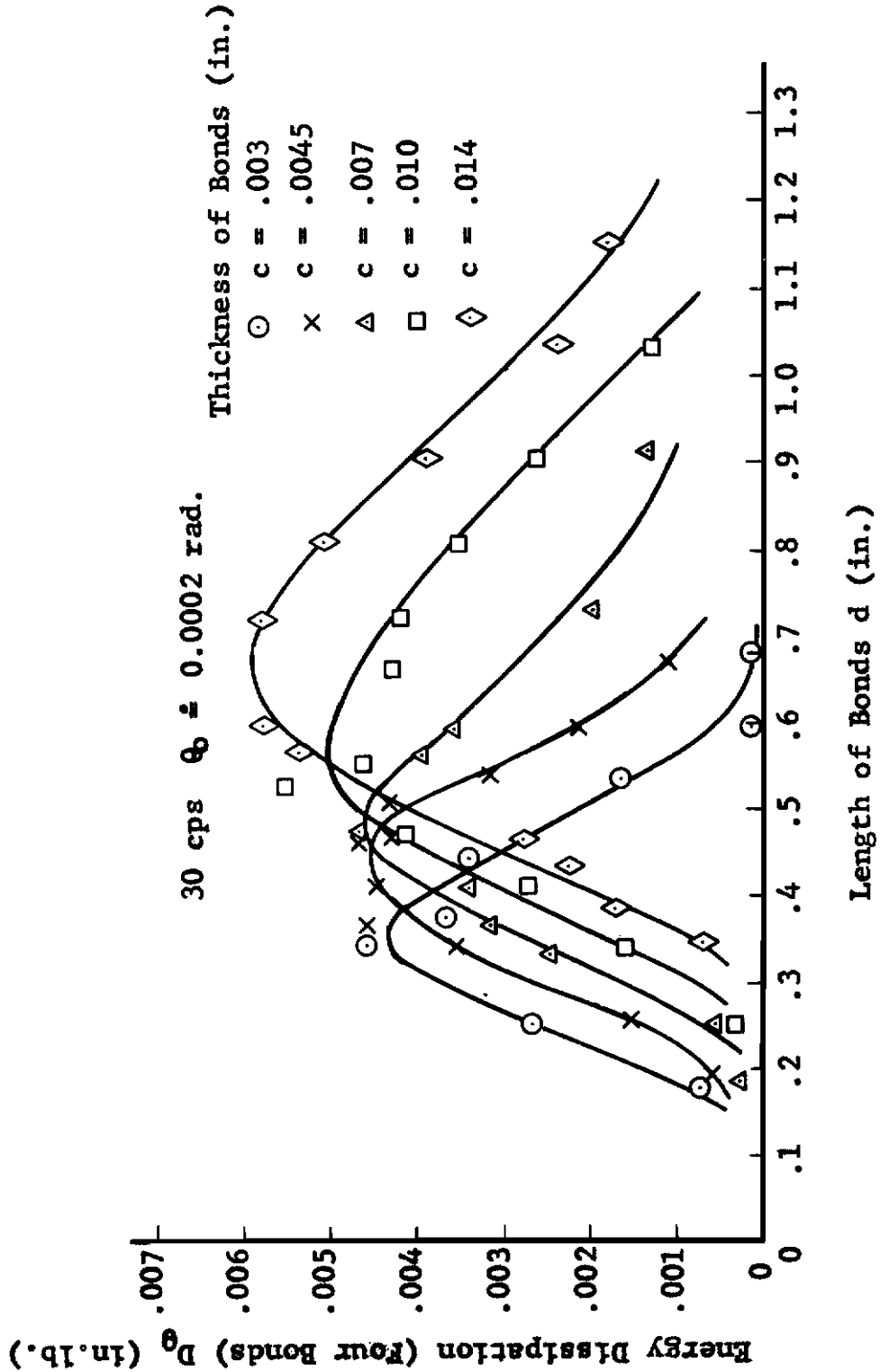


Figure 21 - Rotational Motion Dissipation Characteristics - 30 cps



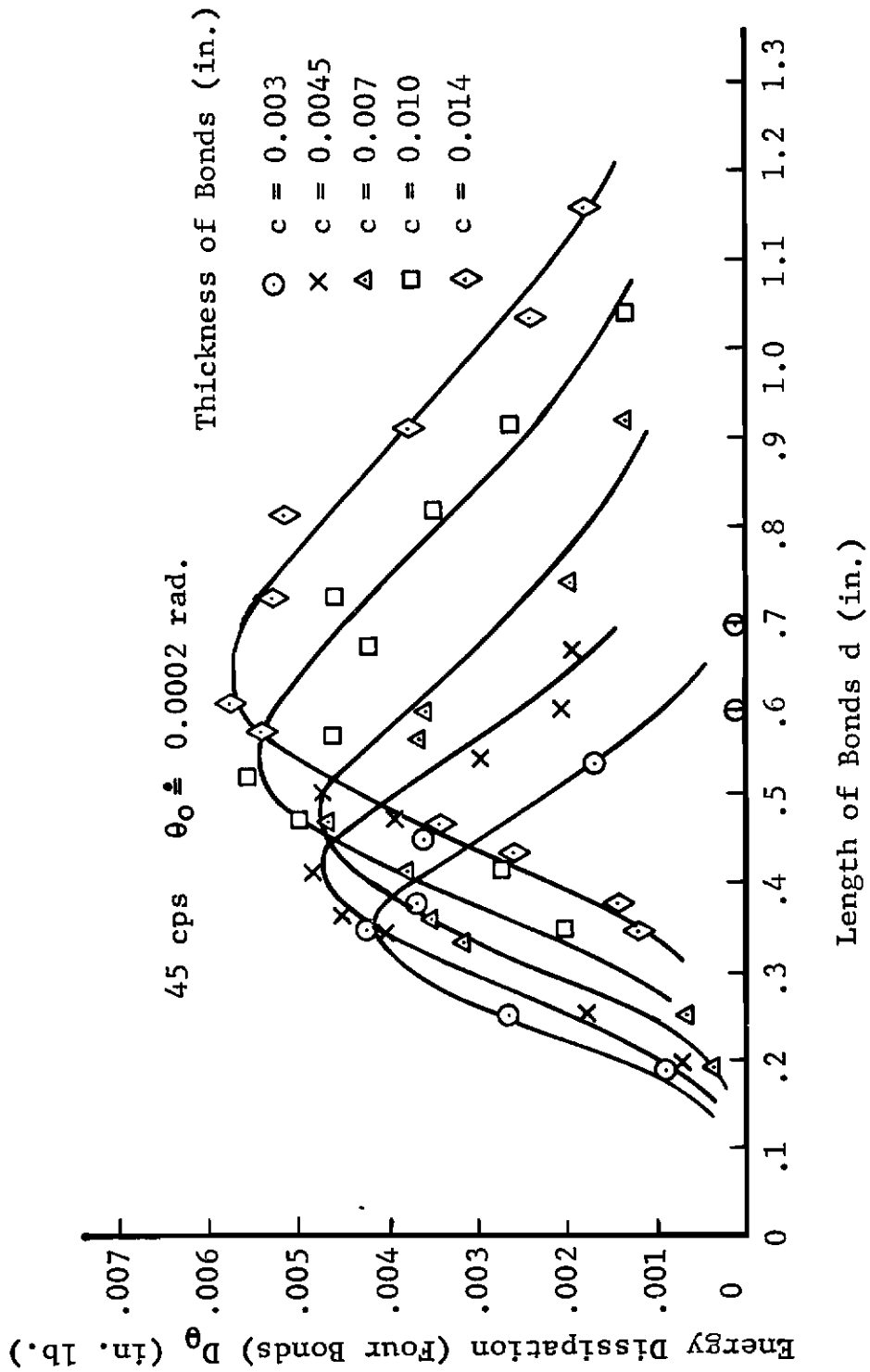


Figure 22 - Rotational Motion Dissipation Characteristics - 45 cps

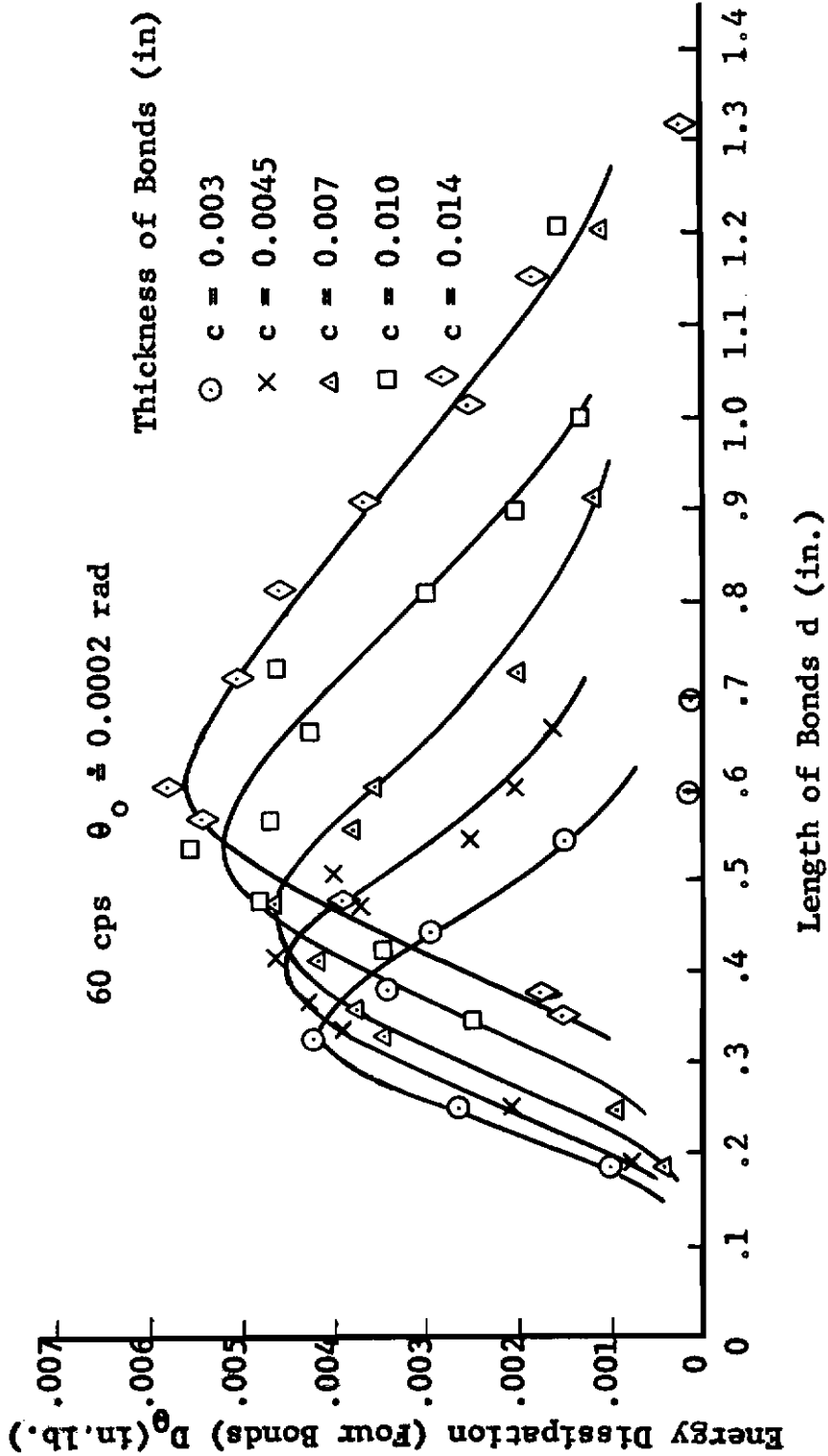


Figure 23 - Rotational Motion Dissipation Characteristics - 60 cps

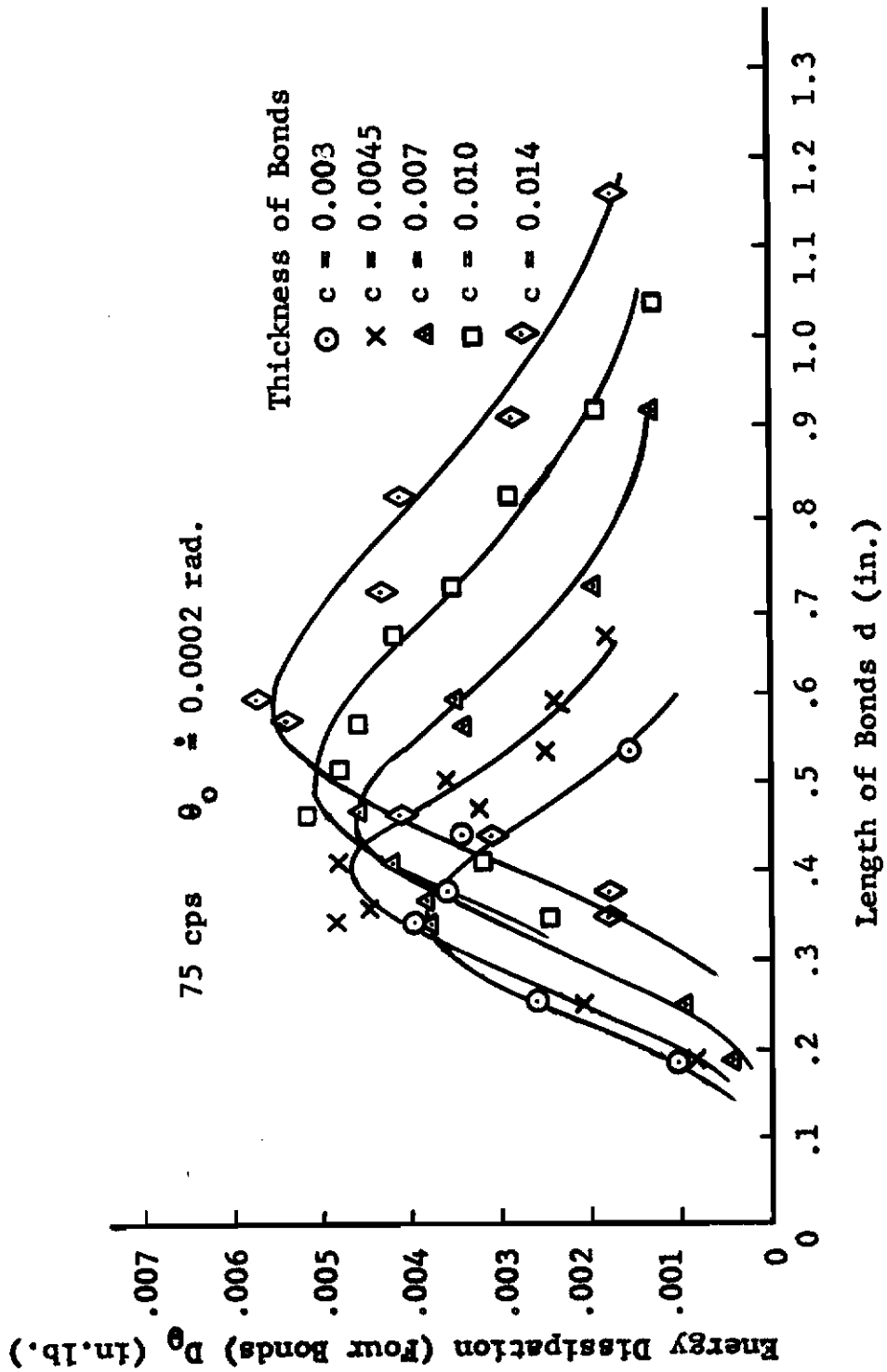


Figure 24 - Rotational Motion Dissipation Characteristics - 75 cps.

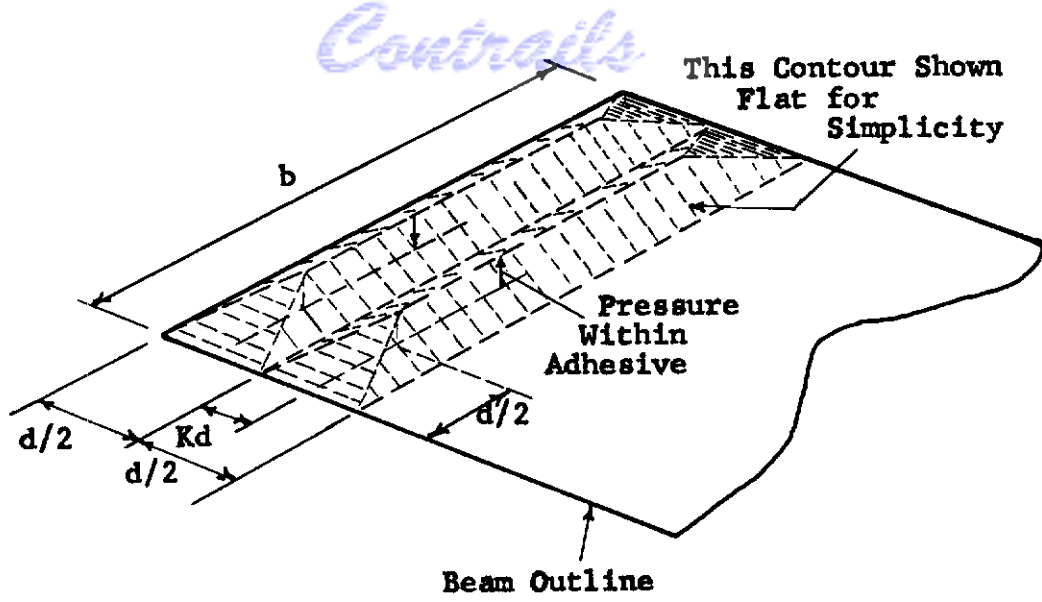


Figure 25 - Approximate Pressure Drop Off At Beam Sides

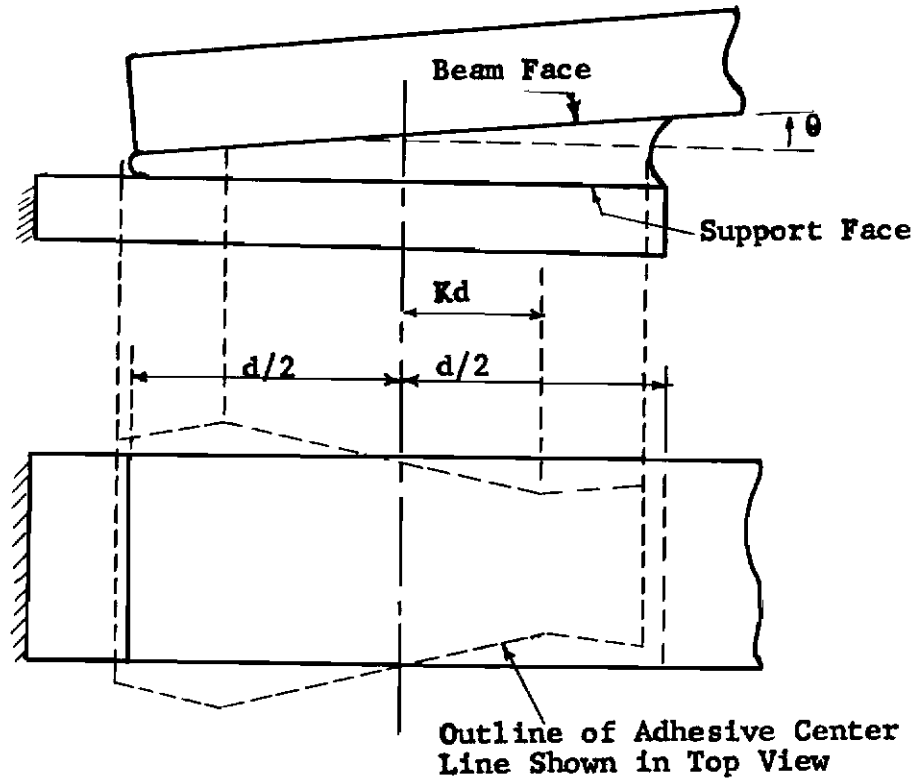
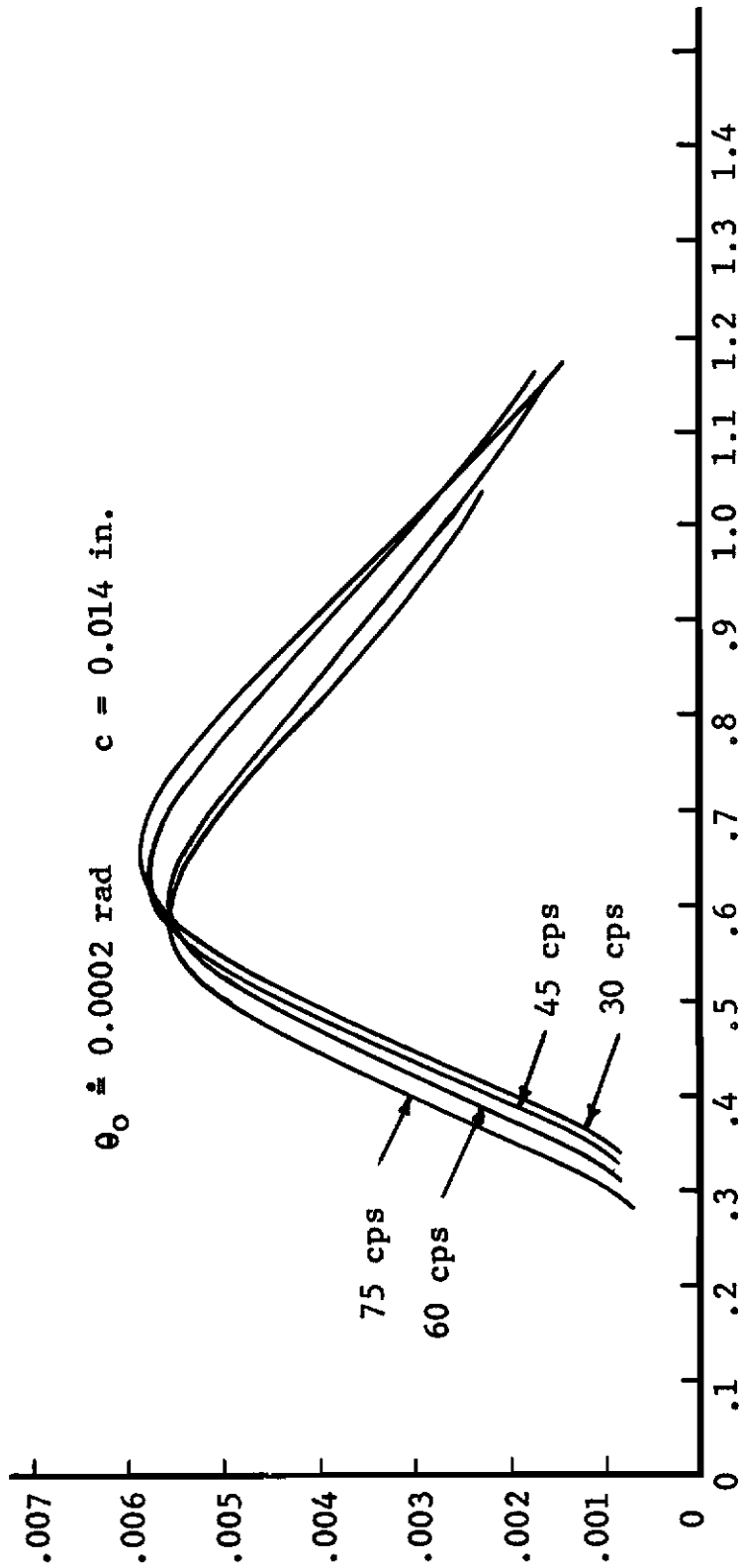


Figure 26- Kinematical Model Incorporating Lateral Adhesive Displacements

Energy Dissipation (Four Bonds)  $D_{\theta}$  (in. lb.)



Length of Bonds  $d$  (in.)

Figure 27 - Frequency Shift of Dissipation

# Contrails

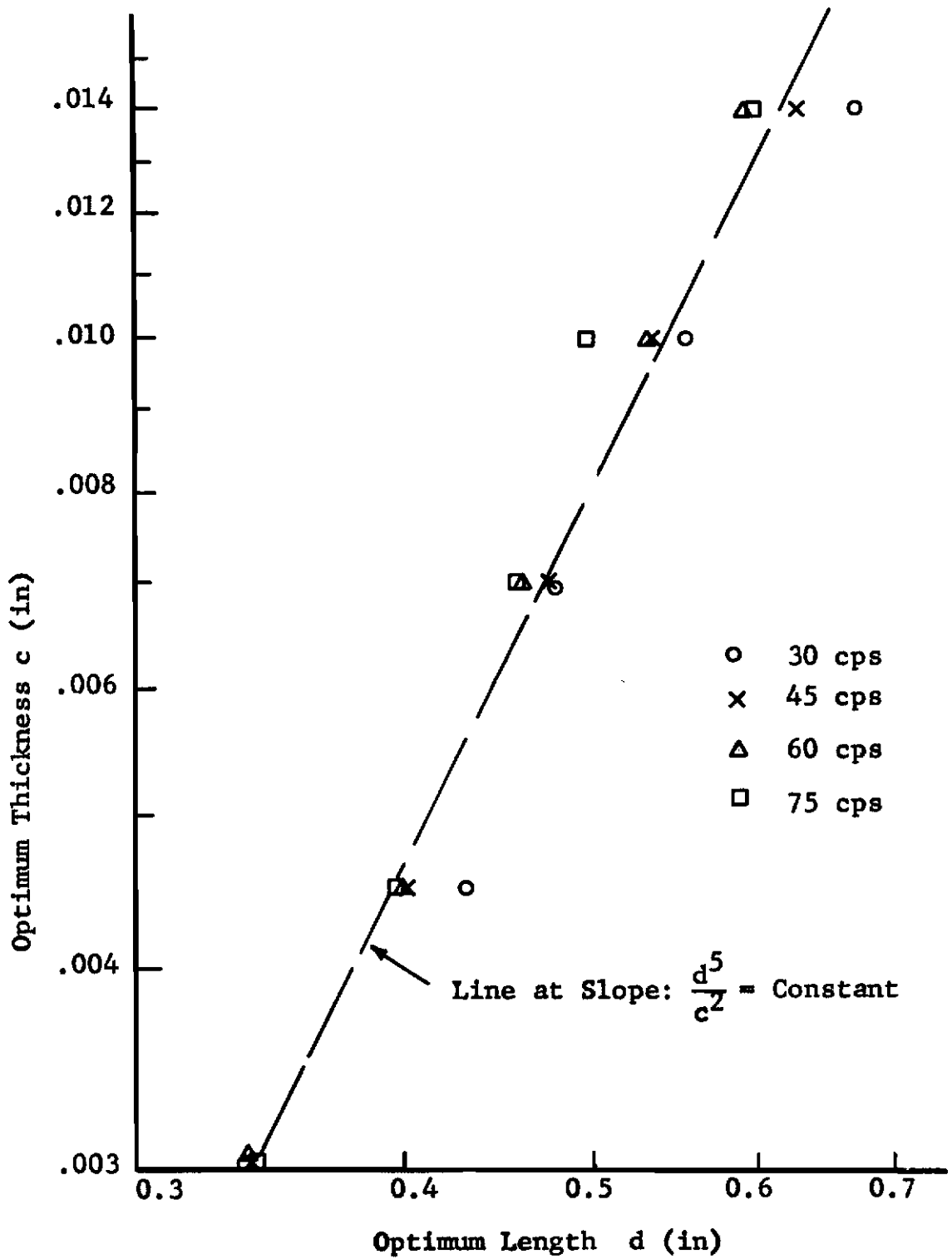


Figure 28 - Combinations of c and d for Maximum Dissipation

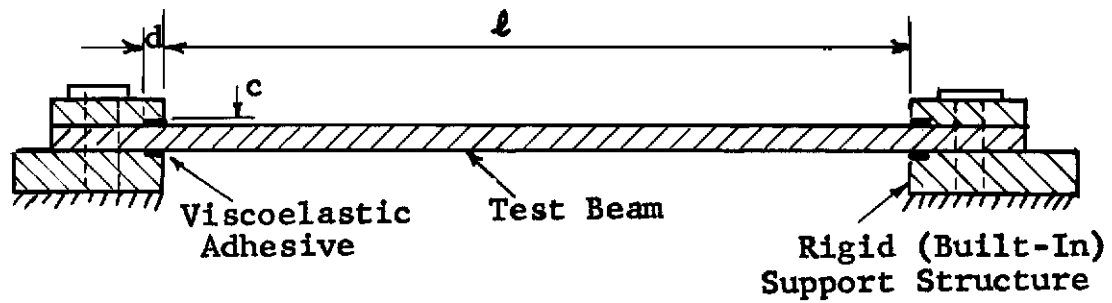


Figure 29 - Flexural Deformation Support Damping Mechanism

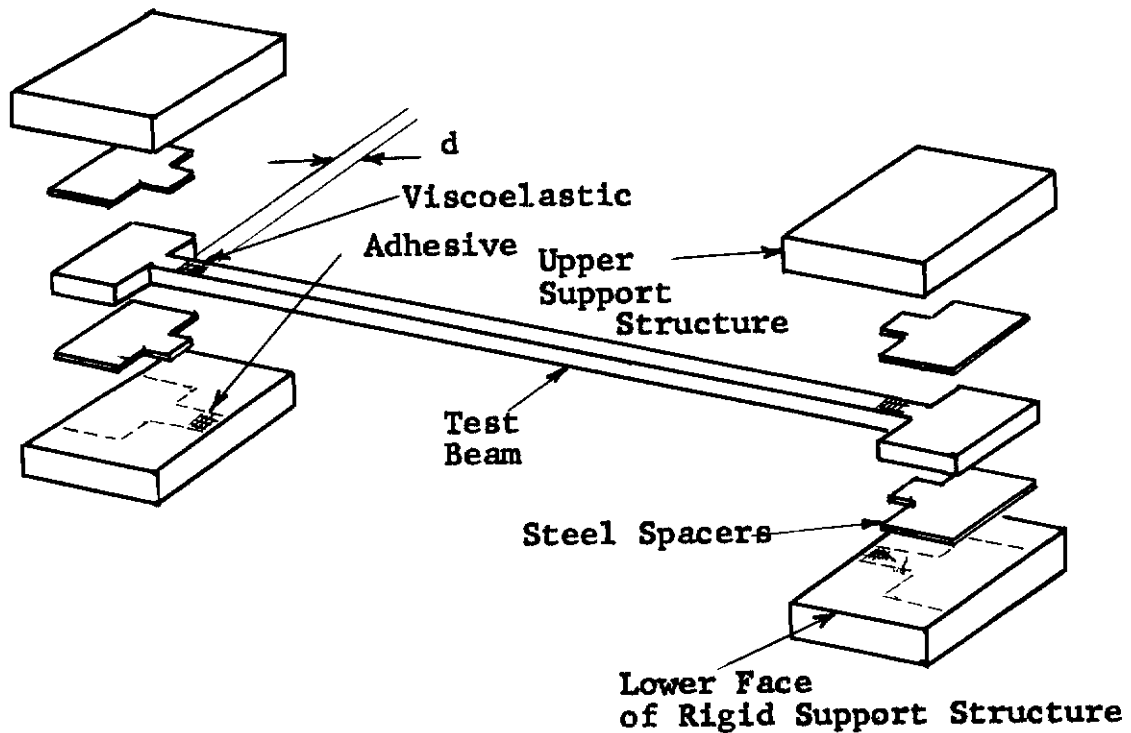


Figure 30 - Exploded View of Set-Up for Flexural Deformation Mechanism

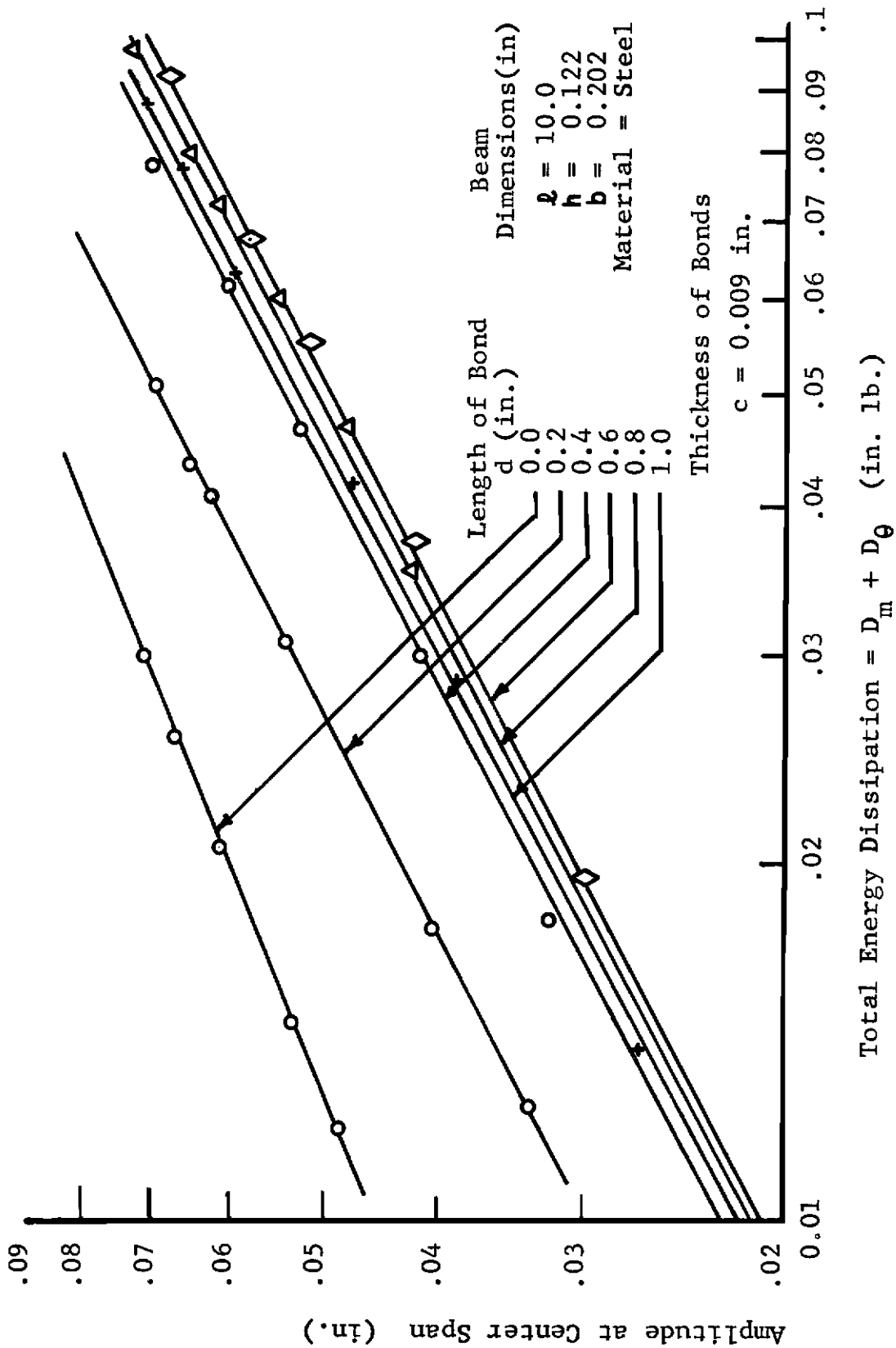


Figure 31 - Typical Results for Flexural Deformation Mechanism



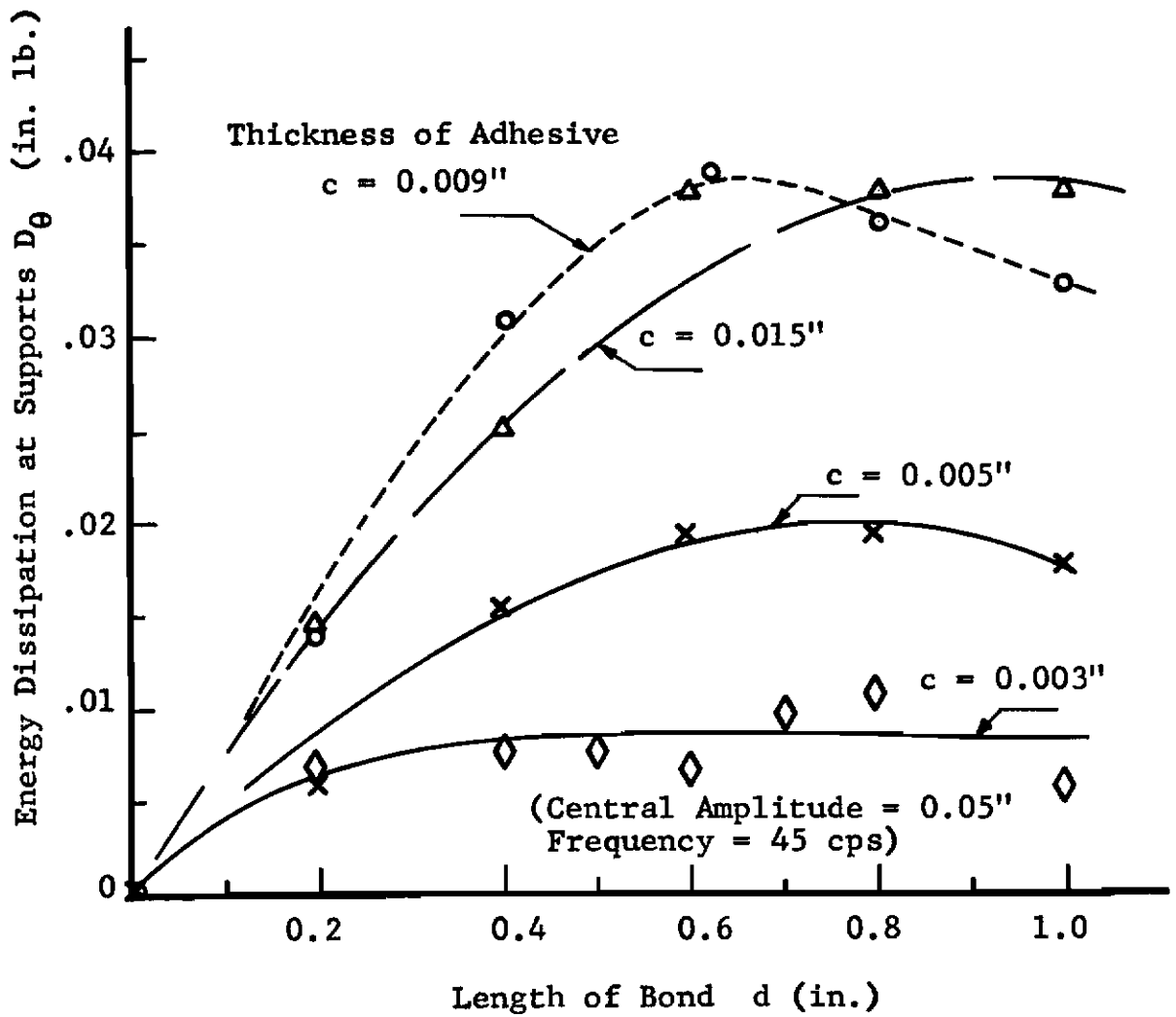


Figure 32 - Influence of Geometry on Flexural Mechanism